A catalogue of stellar diameters and fluxes for mid-infrared interferometry

P. Cruzalèbes, R. Petrov, S. Robbe-Dubois, J Varga, L. Burtscher, F. Allouche, P. Berio, K-H Hofmann, J. Hron, W. Jaffe, et al.

▶ **To cite this version:**

P. Cruzalèbes, R. Petrov, S. Robbe-Dubois, J Varga, L. Burtscher, et al.. A catalogue of stellar diameters and fluxes for mid-infrared interferometry. Monthly Notices of the Royal Astronomical Society, 2019, 490 (3), pp.3158-3176. 10.1093/mnras/stz2803 . hal-02323328

HAL Id: hal-02323328
https://hal.science/hal-02323328

Submitted on 10 Feb 2023

HAL is a multi-disciplinary open access archive for the deposit and dissemination of scientific research documents, whether they are published or not. The documents may come from teaching and research institutions in France or abroad, or from public or private research centers.

L'archive ouverte pluridisciplinaire **HAL**, est destinée au dépôt et à la diffusion de documents scientifiques de niveau recherche, publiés ou non, émanant des établissements d'enseignement et de recherche français ou étrangers, des laboratoires publics ou privés.

Monthly Notices
of the
ROYAL ASTRONOMICAL SOCIETY

MNRAS **490,** 3158–3176 (2019)
Advance Access publication 2019 October 7

doi:10.1093/mnras/stz2803

A catalogue of stellar diameters and fluxes for mid-infrared interferometry★

P. Cruzalèbes,[1]† R. G. Petrov,[1] S. Robbe-Dubois,[1] J. Varga,[2,3] L. Burtscher,[2] F. Allouche,[1] P. Berio,[1] K.-H. Hofmann,[4] J. Hron,[5] W. Jaffe,[2] S. Lagarde,[1] B. Lopez,[1] A. Matter,[1] A. Meilland,[1] K. Meisenheimer,[6] F. Millour[1] and D. Schertl[4]

[1]*Observatoire de la Côte d'Azur, CNRS, Laboratoire Lagrange, Université Côte d'Azur, Parc Valrose, Bât. H. Fizeau, F-06108 Nice, France*
[2]*Leiden Observatory, Leiden University, Niels Bohrweg 2, NL-2333 CA Leiden, the Netherlands*
[3]*Konkoly Observatory, Research Centre for Astronomy and Earth Sciences, Hungarian Academy of Sciences, Konkoly Thege Miklós út 15-17, 1121 Budapest, Hungary*
[4]*Max-Planck-Institut für Radioastronomie, Auf dem Hügel 69, D-53121 Bonn, Germany*
[5]*Department of Astrophysics, University of Vienna, Türkenschanzstrasse 17, A-1180 Vienna, Austria*
[6]*Max-Planck-Institut für Astronomie, Königstuhl 17, D-69117 Heidelberg, Germany*

Accepted 2019 October 1. Received 2019 October 1; in original form 2019 June 9

ABSTRACT

We present the Mid-infrared stellar Diameters and Fluxes compilation Catalogue (MDFC) dedicated to long-baseline interferometry at mid-infrared wavelengths (3–13 μm). It gathers data for half a million stars, i.e. nearly all the stars of the *Hipparcos*-Tycho catalogue whose spectral type is reported in the SIMBAD data base. We cross-match 26 data bases to provide basic information, binarity elements, angular diameter, magnitude and flux in the near and mid-infrared, as well as flags that allow us to identify the potential calibrators. The catalogue covers the entire sky with 465 857 stars, mainly dwarfs and giants from B to M spectral types closer than 18 kpc. The smallest reported values reach 0.16 μJy in *L* and 0.1 μJy in *N* for the flux, and 2 microarcsec for the angular diameter. We build four lists of calibrator candidates for the *L* and *N* bands suitable with the Very Large Telescope Interferometer (VLTI) sub- and main arrays using the MATISSE instrument. We identify 1621 candidates for *L* and 44 candidates for *N* with the Auxiliary Telescopes (ATs), 375 candidates for both bands with the ATs, and 259 candidates for both bands with the Unit Telescopes (UTs). Predominantly cool giants, these sources are small and bright enough to belong to the primary lists of calibrator candidates. In the near future, we plan to measure their angular diameter with 1 per cent accuracy.

Key words: techniques: interferometric – techniques: photometric – catalogues – stars: fundamental parameters – infrared: stars.

1 INTRODUCTION

Modern long-baseline interferometers, such as the ESO-VLTI (Paresce et al. 1996) or the CHARA (ten Brummelaar et al. 2005) arrays, combine the beams of many telescopes (4 for the VLTI, 6 for CHARA) to achieve high angular resolution observations using hectometric baselines. They measure the spectral variation of the correlated flux, visibility, closure phase, differential visibility, and phase in the specific spectral bands.

MIDI, the MID-infrared Interferometric instrument (Leinert et al. 2003), was the first scientific instrument available at the VLTI covering the photometric *N* band (from 8 to 13 μm). Decommissioned in late 2015, it is now replaced by the second-generation instrument MATISSE, the Multi AperTure mid-Infrared SpectroScopic Experiment (Lopez et al. 2014; Allouche et al. 2016; Robbe-Dubois et al. 2018) which operates simultaneously in the three photometric bands: *L* (from 2.8 to 4.2 μm), *M* (from 4.5 to 5 μm), and *N* (from 8 to 13 μm).

Reference targets with well-known angular diameters and hence absolute visibilities are essential to calibrate interferometric observables. Up to now the JMMC Stellar Diameters Catalogue (JSDC,

★ The catalogue is available at CDS via anonymous ftp to cdsarc.u-strasbg.fr (130.79.128.5) or via http://cdsarc.u-strasbg.fr/viz-bin/qcat?II/361. It is also directly downlable in its electronic form at the OCA/MATISSE webpage via https://matisse.oca.eu/foswiki.

† E-mail: pierre.cruzalebes@oca.eu

© 2019 The Author(s)
Published by Oxford University Press on behalf of the Royal Astronomical Society

Downloaded from https://academic.oup.com/mnras/article/490/3/3158/5583026 by guest on 10 February 2023

Cat. II/346; Bourgès et al. 2017) is the largest data base of computed angular diameters in the literature, for nearly half a million stars. It is a basic input of our work. It reports angular diameter estimates of the limb-darkened disc (LDD) and uniform disc (UD) from the *B* to *N* photometric bands. It also reports visible magnitudes from the Tycho-2 Catalogue (Cat. II/259; Høg et al. 2000), near-infrared (NIR) magnitudes from the 2MASS All-Sky Catalogue of Point Sources (Cat. II/246; Cutri et al. 2003), and mid-infrared (MIR) magnitudes from the WISE All-Sky Data Release catalogue (Cat. II/311; Wright et al. 2010). In the framework of the scientific exploitation of the VLTI/MATISSE instrument, we need the most reliable estimates of both the angular diameter and the flux density for MIR wavelengths. As we point out in Section 2.3, a significant number of sources are reported in the WISE catalogue as having spurious MIR flux values (see e.g. Cutri et al. 2012).

The need of reliable flux values leads us to propose a new all-sky catalogue, the Mid-infrared stellar Diameters and Fluxes compilation Catalogue (MDFC), that gathers data from various existing literary sources in order to report in the same table:

(i) angular diameter estimates and measurements;
(ii) flux density measurements and estimates at MIR wavelengths;
(iii) flags identifying the potential interferometric calibrators suitable for the MIR spectral domain.

The main advantages of our catalogue over the JSDC are to supply reliable flux values in the MIR and to report a calibrator selection criterion suitable for this spectral domain.

The paper is divided in five main sections. Section 2 presents the successive steps followed to build the MDFC. Section 3 describes the new flag that allows the identification of the sources that show infrared extended structures (excess, extent, variability). Section 4 presents the content of the MDFC in terms of sky-coverage and distributions in: spectral type, distance, binaries, angular diameter, MIR flux, and calibrators. Section 5 gives clues for selecting calibrators for observations with the VLTI/MATISSE instrument. Section 6 shows an example of application of the catalogue with the building of the primary lists of calibrators for VLTI/MATISSE.

2 BUILDING THE CATALOGUE

To build the MDFC:

(i) we use as input the JDSC catalogue which reports angular diameter estimates with their uncertainties;
(ii) we complete the diameter data with those of three other diameter catalogues providing measurements and other estimates;
(iii) we include the basic data (including astrometric binarity);
(iv) we compile MIR flux data reported in 12 other photometric catalogues;
(v) we add a new flag that identifies the stars showing MIR features (excess, extent, variability).

2.1 Input catalogues for the angular diameter

Since the JSDC is the most complete and up-to-date catalogue used for visible/infrared interferometric calibration, we use it as primary input to build the MDFC. The JSDC contains 465 877 entries (among which we have identified and deleted 272 duplicates) and reports estimates of LDD and UD angular diameters from the *B* to *N* spectrophotometric bands, providing a flag for each star indicating a degree of confidence in choosing it as a calibrator for optical long-baseline interferometry (OLBI). We complete the diameter data with the values reported in the three following smaller catalogues, also widely used for interferometric calibration:

(i) the JMDC, the JMMC Measured Stellar Diameters Catalogue (Cat. II/345; Duvert 2016), that reports 1554 direct measurements of UD and LDD diameters for 566 different stars, made with 'direct' techniques (optical interferometry, intensity interferometry, and lunar occultations) from the visible to the MIR wavelengths;
(ii) the VLTI/MIDI list of calibrator candidates, which reports 403 estimates of LDD diameter with fitted effective temperatures obtained from Verhoelst (2005);
(iii) the Cohen's list of spectrophotometric standards, which reports 422 estimates of LDD diameter derived from calibrated spectral templates (Cohen et al. 1999, Table 4).

The aggregating of these three small catalogues with the JSDC leads to a total of 465 857 stars that have at least one angular diameter estimate or measurement reported at visible and/or infrared wavelengths. Note that if many diameter values are available for a given star, we suggest to favour the value given by the JSDC primary catalogue. Large discrepancies between angular diameter estimates for a given source may indicate that this source is a bad calibrator. The final catalogue includes nearly all the stars of the *Hipparcos*-Tycho catalogue (Cat. I/239; ESA 1997) whose spectral type is reported in the SIMBAD data base (Wenger et al. 2000). All entries of the catalogue have *H* and *K* magnitudes reported in 2MASS.

2.2 Reporting basic, fundamental, and binarity data

Spectral type and equatorial coordinates are taken from the SIMBAD data base. Binarity observational data (astrometric) are reported from the Washington Double Star Catalogue (Cat. B/wds; Mason et al. 2001).

We report the effective temperature and the stellar physical radius from the *Gaia* DR2 catalogue (Cat. I/345/gaia2; Gaia Collaboration 2018), and the distance from the complement of the *Gaia* DR2 catalogue (Cat. I/347/gaia2dis; Bailer-Jones et al. 2018). From the radius to distance ratio we report another estimate of the LDD diameter.[1]

2.3 Reporting and merging MIR flux data

Beside basic and angular diameter data, our catalogue also reports flux data in the NIR and MIR. The *J*, *H*, and *K* magnitudes are reported in the 2MASS Catalogue. For a substantial number of stars (mainly IR-bright stars), we notice that the flux measurements in the MIR photometric bands may vary significantly from one catalogue to the other. In the example of the M3II star 72 Leo shown in Fig. 1, we note some spurious flux values reported in the MIR bands. The wide dispersion of the measurements observed for these sources is greater than the spread in flux caused by the width of the spectral band. Under the blackbody model assumption with $T_{\rm eff} = 4000$ K,

[1]The values of effective temperature and radius reported in the *Gaia* DR2 catalogue were determined only from the three broad-band photometric measurements with *Gaia*. The strong degeneracy between $T_{\rm eff}$ and extinction/reddening when using the broad-band photometry necessitates strong assumptions in order to estimate their values (see e.g. Casagrande & VandenBerg 2018). One should thus be very careful in using these astrophysical parameters and refer to the papers and online documentation for guidance.

Downloaded from https://academic.oup.com/mnras/article/490/3/3158/5583026 by guest on 10 February 2023

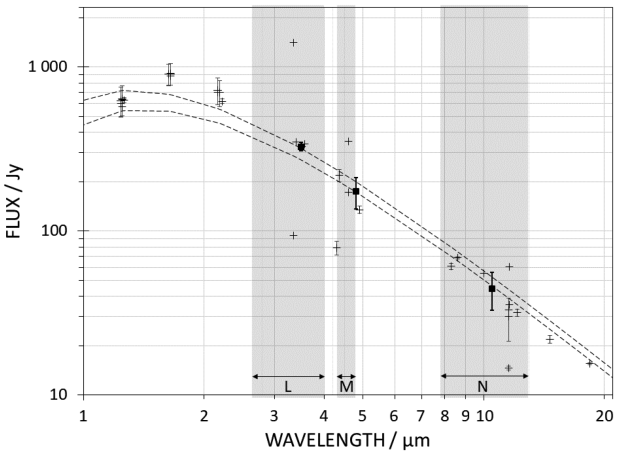

Figure 1. Flux measurements between 1 and 20 µm reported in the VizieR Photometry viewer for the M3II star 72 Leo in a radius of 5 arcsec around its central position. The spectral domains covered by the VLTI/MATISSE are shaded in grey. The three black squares are the median values reported in our catalogue with their statistical dispersion. The upper and lower dashed curves are the SEDs given by the blackbody model with the MIDI and *Gaia* DR2 parameters, respectively.

this spread in flux does not exceed 43 per cent for the *L* band (2.8–4.2 µm), 15 per cent for the *M* band (4.5–5 µm), and 58 per cent for the *N* band (8–13 µm).

For each star, we compile the flux values reported in various catalogues. Our goal is to report an approximate but reliable final value of the flux density for each MIR photometric band, without any use of modelling the in-band flux based on the measured photometry. If more than two flux values are reported for each MIR band, we compute the median value (*F*), less sensitive to spurious values than the sample mean. The reliability of the final flux value is estimated by the median absolute deviation from the median (*MAD*), which gives a robust estimate of the statistical scatter. If only two flux values are reported, we compute the mean value and the range, i.e. the difference between the maximum and the minimum values. If one of those two values is irrelevant, the large value of the range is an indication of the irrelevance of the final flux value. If only one flux value is reported, no associated dispersion is reported.

The flux density measurements are reported in:

(i) the AllWISE survey (Cat. II/328; Wright et al. 2010, 747 million sources covering 99.86 per cent of the entire sky) for the *WISE*/*W*1, *W*2, and *W*3 filters, with flux senstivities better than 0.08, 0.11, and 1 mJy, respectively. Since the original WISE catalogue (563 million sources) may have better photometric information for objects brighter than the saturation limit for the *W*1 and *W*2 filters, the *WISE* flux measurements supersede the AllWISE measurements for magnitudes $[W1] < 8$ and $[W2] < 7$ (see Cutri et al. 2013);

(ii) the GLIMPSE Source Catalogue (Cat. II/293; Benjamin et al. 2003, 104 million sources covering approximately 220 square degrees for $|l| \leq 65°$– galactic longitude – and $|b| \leq 1°$– galactic latitude) for the 3.6-, 4.5-, and 8-µm *Spitzer*-IRAC bands, with flux sensitivities better than 0.6, 0.4, and 10 mJy, respectively;

(iii) the AKARI/IRC All-Sky Survey Point Source Catalogue (Cat. II/297; Ishihara et al. 2010, 870 973 sources covering more than 90 per cent of the entire sky) for the AKARI/S9W filter with flux sensitivity better than 20 mJy;

Table 1. Characteristics of the broad-band filters (– indicates an undefined value) used to report flux in the bands: *L* (top), *M* (middle), and *N* (bottom).

Catalogue	Filter	Isophotal wavel. (µm)	Zero-mag. flux (Jy)	Angular Resol.
WISE	*W*1	3.35	310	6.1 arcsec
MIDI	SAAO/L	3.5	294	34 arcsec
JP11	L	3.5	288	–
DIRBE	F3.5	3.5	282	0.7°
GLIMPSE	IRAC3.6	3.6	281	1.7 arcsec
MSX	B1	4.29	195	18.3 arcsec
MSX	B2	4.35	189	18.3 arcsec
GLIMPSE	IRAC4.5	4.5	180	1.7 arcsec
WISE	W2	4.6	172	6.4 arcsec
DIRBE	F4.9	4.9	153	0.7°
JP11	M	5.0	158	–
GLIMPSE	IRAC8	7.87	64.1	2 arcsec
MSX	A	8.28	58.5	18.3 arcsec
AKARI	S9W	9.0	56.3	5.5 arcsec
10 µm-CAT.	10 µm	10.0	30.0	–
JP11	N	10.2	43.0	–
IRAS	F12	11.43	28.3	0.5 arcmin
WISE	W3	11.56	31.7	6.5 arcsec
DIRBE	F12	12.0	29.0	0.7°
MSX	C	12.13	26.1	18.3 arcsec

(iv) the MSX6C Infrared Point Source Catalogue (Cat. V/114; Egan, Price & Kraemer 2003, 431 711 sources for $|b| \leq 6°$ and 10 168 sources for $|b| > 6°$, covering a total of 10 per cent of the entire sky) for the *A*-, *B*1-, *B*2-, and *C*-MSX bands, with flux sensitivity reaching 0.1, 10, 6, and 1.1 Jy, respectively;

(v) the *IRAS* PSC/FSC Combined Catalogue (Cat. II/338; Abrahamyan, Mickaelian & Knyazyan 2015, 345 162 sources covering the entire sky) for the *IRAS*/12 filter with flux sensitivity better than 0.25 Jy. The *IRAS*/12 values are completed with the values of the *IRAS* Faint Source Catalogue (Cat. II/156A; Moshir et al. 1990, 173 044 sources for $|b| > 10°$) with flux sensitivity better than 0.1 Jy, and those of the Point Sources Catalogue (Cat. II/125; Helou & Walker 1988, 245 889 sources covering the entire sky) with flux sensitivity better than 0.25 Jy;

(vi) the *COBE* DIRBE Point Source Catalogue (Cat. J/ApJS/154/673; Smith, Price & Baker 2004, 11 788 sources covering 85 per cent of the entire sky) for the F3.5, F4.9, and F12 *COBE*-DIRBE filters, with flux sensitivities at high galactic latitudes ($|b| > 5°$) better than 60, 50, and 90 Jy, respectively;

(vii) the *UBVRIJKLMNH* Photoelectric Catalogue (Cat. II/7A; Morel & Magnenat 1978, compiling reported measurements of 4494 sources published up to 1978) for the *L*-, *M*-, and *N*-Johnson filters;

(viii) the Catalogue of 10-micron Celestial Objects (Cat. II/53; Hall 1974, compiling reported measurements of 647 sources published between 1964 and 1973) for $\lambda = 10$ µm.

The conversion of MIR magnitudes to fluxes is done using the zero-magnitude flux values given in Table 1, which also gives the angular resolution in each filter used with the different surveys.

In addition to the photometric measurements reported in the catalogues listed here above, we use flux estimations that we average for each MIR spectral band, reported in:

(i) the VLTI/MIDI list of calibrator candidates (403 sources) for the SAAO/*L* and *IRAS*/12 filters;

Downloaded from https://academic.oup.com/mnras/article/490/3/3158/5583026 by guest on 10 February 2023

Table 2. Number of entries for each number of reported individual flux values for each band.

# of flux values	In *L*	In *M*	In *N*
0	102	100	107
1	33 683	33 627	31 781
2	412 467	411 345	270 212
3	19 058	19 417	85 130
4	487	1028	65 802
5	60	288	9179
6	0	52	3047
7	0	0	529
8	0	0	64
9	0	0	6

(ii) the tables of parameters and IR excesses of *Gaia* DR1 stars (Cat. J/MNRAS/471/770; McDonald, Zijlstra & Watson 2017, 1.47 million sources covering the entire sky) for the *WISE*/*W*1, *WISE*/*W*2, *WISE*/*W*3, AKARI/S9W, and *IRAS*/12 filters;

(iii) the blackbody model for $\lambda = 3.5$, 4.8, and 10.5 μm, using the values of effective temperature and angular diameter reported in the VLTI/MIDI list and the *Gaia* DR2;

(iv) the complete set of Cohen's standards (435 sources) for $\lambda = 10.7$ μm, downloadable from the Gemini Observatory Website (with the link given in Appendix A).

The values used to compute the final flux values with their statistical dispersions are reported in: 6 databases for the *L* band; 8 databases for the *M* band; and 12 data bases for the *N* band. Table 2 gives the number of entries as a function of the number of flux values reported in each MIR band. In our catalogue, 93 per cent of the entries have at least 2 flux values reported in each band, while 4 per cent have at least 3 flux values in *L* and *M*, 35 per cent in *N*. The maximum number of flux values effectively used are: 5 for the *L* band, 6 for the *M* band, and 9 for the *N* band.

It should be noted that the merging of individual flux data obtained with such a different angular resolution (from 1.7 arcsec for GLIMPSE to 0.7° for DIRBE) may cause source confusion. Flux values may be slightly overestimated with observing beams including numerous unresolved sources and their circumstellar environment.

For the star 72 Leo taken as an example in Fig. 1, the median flux values (drawn as black squares) are $F_L = 327$ Jy, $F_M = 174$ Jy, and $F_N = 44$ Jy, computed with 5 individual values for *L*, 6 values for *M*, and 8 values for *N* (see Table 3 for details). The *MAD* values are 19 Jy for *L*, 37 Jy for *M*, and 11.5 Jy for *N*. We observe that the median values match the mean SED (spectral energy distribution), falling between the SEDs of the blackbody model with $\phi = 5.9$ mas, $T_{\rm eff} = 3900$ K (*Gaia* DR2 values), and with $\phi = 5.8$ mas, $T_{\rm eff} = 3600$ K (MIDI values). The calculation of the mean and standard deviation of the flux would give: $\bar{F}_L = 281 \pm 105$ Jy; $\bar{F}_M = 163 \pm 49$ Jy; and $\bar{F}_N = 47 \pm 13$ Jy. Based on the *MAD* assessment, the average uncertainty that we report in our catalogue is lower than the standard deviation σ, since outliers can heavily influence σ, while deviations of a small number of outliers are irrelevant in the *MAD*. Note that for a normal distribution, *MAD* is related to σ as $MAD \sim 0.67\sigma$.

Appendix A lists the complete set of data bases used to build our catalogue, with the number of entries reported in each of them and the references.

Table 3. Flux values reported in our catalogue for 72 Leo (– indicates that no value is reported, 'BB' stands for 'blackbody') in the 3 bands: *L* (top), *M* (middle), and *N* (bottom).

Catalogue	Wavelength (μm)	Flux (Jy)
WISE_W1	3.35	95.1
BB_MIDI	3.5	307.2
BB_*Gaia*	3.5	328.1
JP11_L	3.5	349.5
DIRBE_F3.5	3.5	326.6
GLIMPSE_IRAC3.6	3.6	–
MSX_*B*1	4.29	78.9
MSX_*B*2	4.35	218.2
GLIMPSE_IRAC4.5	4.5	–
WISE_W2	4.6	173.1
BB_MIDI	4.8	173.9
BB_*Gaia*	4.8	197.8
DIRBE_F4.9	4.9	136.9
JP11_M	5.0	–
GLIMPSE_IRAC8	7.87	–
MSX_A	8.28	60.9
AKARI_S9W	9.0	68.5
10 μm-CAT	10.0	49.5
JP11_N	10.2	–
BB_MIDI	10.5	41.1
BB_*Gaia*	10.5	44.4
COHEN	10.7	–
*IRAS*_F12	11.43	–
*WISE_W*3	11.56	33.0
DIRBE_F12	12.0	34.2
MSX_*C*	12.13	31.8

3 IDENTIFYING THE STARS WITH IR EXTENDED FEATURES

The JSDC reports a 3-bit flag, called 'CalFlag', which identifies the stars that should not be used as interferometric calibrators because of:

(i) the uncertain estimation of their reconstructed angular diameter, with $\chi^2 > 5$ (see appendix A.2 of Chelli et al. 2016);

(ii) their close binarity, with $\varepsilon < 1$ arcsec reported in WDS;

(iii) their suspect Object Type in SIMBAD which signals a possible binarity or pulsating stars.

Beside 'CalFlag', we define a new 3-bit flag, called 'IRflag'. This new flag identifies the stars that show probable extended features at MIR wavelengths revealed by their photometric excess, extent, and/or variability.

3.1 Tagging the IR-excess

The first bit of IRflag is set if the star shows an IR-excess, identified thanks to the values of:

(i) the [*K*-*W*4] colour index[2] defined in 3 different [*J*-*H*] parts (according to Wu et al. 2013): (i) [*K*-*W*4] ≥ 0.26 for [*J*-*H*] ≤ 0.1; (ii) [*K*-*W*4] ≥ 0.21 for 0.1 < [*J*-*H*] ≤ 0.3; and (iii) [*K*-*W*4] ≥ 0.22 for [*J*-*H*] > 0.3;

[2][W4] means the magnitude at 22.1 μm reported in the *WISE* All-Sky Data Release (*W*4 filter).

Downloaded from https://academic.oup.com/mnras/article/490/3/3158/5583026 by guest on 10 February 2023

(ii) the overall MIR-excess statistic X_{MIR} reported by McDonald et al. (2017) for a large sample of Tycho-2 and *Hipparcos* stars with distances from *Gaia* DR1, following the IR-excess criterion: $X_{MIR} > 1.15 + A_V/100$, where A_V is the optical extinction.

It should be noted, however, that sources tagged as IR-excess stars in our catalogue might also include good candidates wrongly tagged with these criteria, since the IR-excess could also be from nearby bright stars or background sources.

3.2 Tagging the IR-extent

The second bit of IRflag is set if the star is far-extended in the IR (at angular scale of several arcseconds), indicated by the extent flags reported in the 2 catalogues WISE/AllWISE and AKARI. We consider the source as possibly non-extended if it has:

(i) the *WISE* extent flag = 0, meaning that: (i) the source shape is consistent with a point source (FWHM = 6.1 arcsec in *L* and *M*, 6.5 arcsec in *N*), with a goodness-of-fit value of the photometric profile fit < 3 in all bands; and (ii) that the source is not associated with or superimposed on an NIR source of the 2MASS Extended Source Catalogue; or
(ii) the AKARI extent flag = 0. Unity flag means that the average of the radius along the major and minor axes of the source extent estimated with SEXTRACTOR is > 15.6 arcsec, more extended than the PSF in the *S*9*W* band (FWHM = 5.5 arcsec).

It should be noted, however, that very bright point sources of our catalogue might also appear as extended with these criteria. Moreover, the lack of information on circumstellar extent at the subarcsecond scale (below 1 arcsec) does not warranty the source to be free from a close circumstellar environment (better revealed by the IR-excess).

3.3 Tagging the MIR variability

The third (and last) bit of IRflag is set if the star is a likely variable in the MIR, identified by the variability flags reported in the *WISE*/AllWISE catalogues, the MSX6C Infrared Point Source Catalogue, the *IRAS* Point Sources Catalogue, and the 10-micron Catalogue. We consider the source as a likely variable if it:

(i) is tagged as a likely variable in at least one of the *WISE* filters *W*1, *W*2, or i3 (variability flag of '7' or '8'); or
(ii) has the variability flag = 1 in at least one of the MSX filters *B*1, *B*2, *C*, or *A*; or
(iii) has the likelihood of variability >90 per cent in the *IRAS*/12 filter; or
(iv) is tagged as a variable star for $\lambda = 10$ μm.

Stars fulfilling none of those criteria listed here above are unlikely variable. It should be noted, however, that sources with false-positive variability reported in our catalogue might also be considered as likely variable with those criteria.

4 RESULTS

Appendix B gives the meaning of the columns of our catalogue. The description is presented as a three-column table with the following elements:

(i) a label or column header;
(ii) the unit in which the value is expressed; and
(iii) a short explanation of the contents of the column.

Our catalogue is available at CDS via anonymous ftp to cdsarc.u-strasbg.fr (130.79.128.5) or via http://cdsarc.u-strasbg.fr/viz-bin/qcat?II/361. It is also directly downlable in its electronic form at the OCA/MATISSE webpage via https://matisse.oca.eu/foswiki.[3] It contains a total of 465 857 entries covering the entire sky, including 201 200 'pure' calibrators (with null CalFlag and IRflag), and 28 003 binaries reported in the WDS. Only 102 entries have no individual flux measurement or even estimate reported in the *L* band, 100 in the *M* band, and 107 in the *N* band, while 88 entries have no flux value reported in any of these three bands. The number of sources visible from the ESO-Paranal Observatory reaches 371 333, i.e. 80 per cent of the catalogue entries, including 156 602 'pure' calibrators.

4.1 Sky coverage

Fig. 2 shows the all-sky density map of all the entries of the catalogue in galactic coordinates. The overdensities are distributed along the Milky Way, highlighted by the contour lines. The density in galactic longitude is higher than 14 700 entries per bin of 1 h.

4.2 Spectral and luminosity class distribution

Fig. 3 shows the distribution of spectral and luminosity classes of the entries of the catalogue. About 9 per cent of catalogue entries have spectral class O or B; 88 per cent have spectral class A, F, G, or K; 3 per cent have spectral class M, R, N, S, C, or D. Only one entry of the catalogue (BD+472769, an eruptive variable star) has no spectral type reported in SIMBAD. About 2 per cent of catalogue entries have luminosity class I or II; 35 per cent have luminosity class III, IV, or V; 0.07 per cent have luminosity class VI or VII; and 63 per cent of the entries have no luminosity class reported in SIMBAD.

4.3 Distance distribution

Fig. 4 shows the distribution of the geometric distance from Bailer-Jones et al. (2018):

(i) lower quartile distance: 215 pc;
(ii) median distance: 400 pc;
(iii) upper quartile distance: 690 pc.

About 6 per cent of the entries have $D < 100$ pc, and only 1 per cent have $D < 43$ pc. The most distant source of the catalogue is located at 18.4 kpc (BM VII 9; A1IIIe Spectral Type). We want to stress that the distance values at the kpc scale from the *Gaia* DR2 must be used with caution (see e.g. Luri et al. 2018).

4.4 Binaries distribution

Fig. 5 shows the distribution in angular separation (ε) of the 28 003 astrometric binaries reported in the catalogue from the WDS:

(i) lower quartile separation: 2 arcsec;
(ii) median separation: 21 arcsec;
(iii) upper quartile separation: 77 arcsec.

Only 2 per cent of the entries have $\varepsilon < 0.1$ arcsec.

According to their angular separation, we divide the astrometric binaries contained in our catalogue in three different subsets:

[3] https://matisse.oca.eu/foswiki/pub/Main/TheMid-infraredStellarDiametersAndFluxesCompilationCatalogue(MDFC)/mdfc-v10.zip.

Downloaded from https://academic.oup.com/mnras/article/490/3/3158/5583026 by guest on 10 February 2023

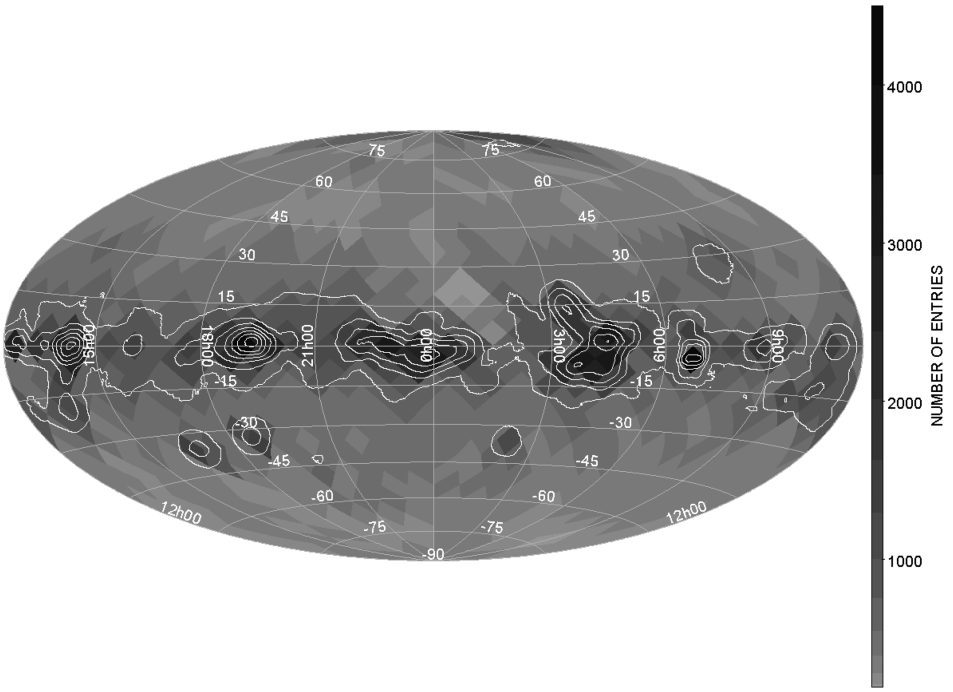

Figure 2. All-sky density map of the whole catalogue, in galactic coordinates.

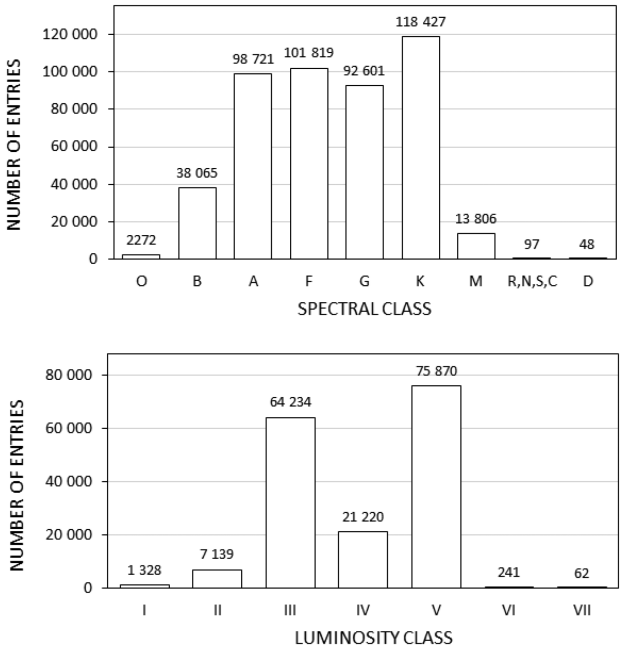

Figure 3. Distribution in spectral (top) and luminosity (bottom) class for the entries of our catalogue.

(i) The wide binaries: $\varepsilon \geq 1$ arcsec.
(ii) The intermediate binaries: 0.4 arcsec $\leq \varepsilon < 1$ arcsec.
(iii) The close binaries: $\varepsilon < 0.4$ arcsec.

Table 4 gives the number of entries for each subclass of the binaries.

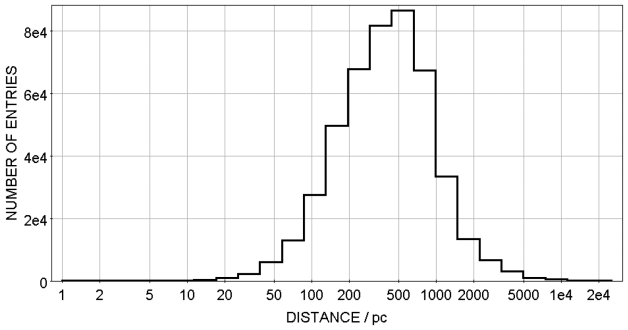

Figure 4. Distribution in geometric distance computed by Bailer-Jones et al. (2018) for the entries of our catalogue.

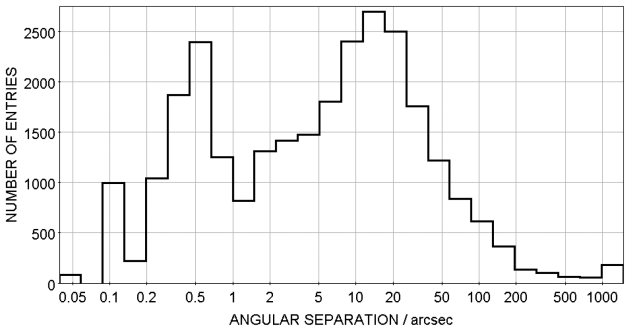

Figure 5. Distribution in angular separation of the sources of our catalogue identified as binaries in the WDS.

Downloaded from https://academic.oup.com/mnras/article/490/3/3158/5583026 by guest on 10 February 2023

Table 4. Number of entries for each binaries subset (see Section 4.4 for the definition of the subsets, based on the WDS).

Subset	# of entries
Wide binaries	19 895
Intermediate binaries	4478
Close binaries	3630

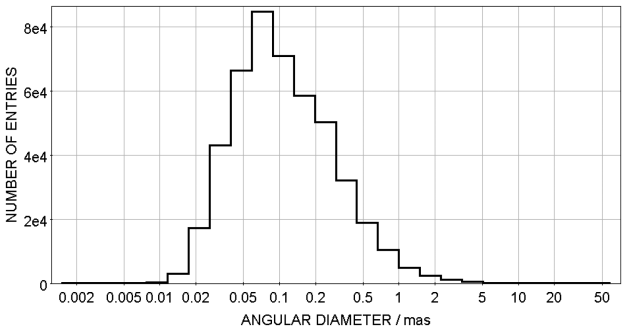

Figure 6. Distribution in angular diameter reported in the JSDC for the entries of our catalogue.

Table 5. Number of entries for each angular diameter subset (see Section 4.5 for the definition of the subsets, based on the JSDC).

Subset	# of entries
Large	5
Medium size	74
Small	762
Point like	464 763

4.5 Angular diameter distribution

Fig. 6 shows the distribution of the LDD diameter (ϕ) computed by Chelli et al. (2016) and reported in the JSDC:

(i) lower quartile diameter: 0.05 mas;
(ii) median diameter: 0.1 mas;
(iii) upper quartile diameter: 0.2 mas.

Only 2 per cent of the entries have $\phi > 1$ mas.

According to their angular diameter, we divide the stellar sources contained in our catalogue into four different subsets:

(i) the 'large' sources, fully resolved in L and N with a 130-m projected interferometric baselength: $\phi \geq 20$ mas;
(ii) the 'medium-size' sources, fully resolved in L and partially resolved in N: $7 \leq \phi < 20$ mas;
(iii) the 'small' sources, partially resolved in L and unresolved in N: $3 \leq \phi < 7$ mas;
(iv) the 'point-like' sources, unresolved in L and N: $\phi < 3$ mas.

Table 5 gives the number of entries for each subclass of angular diameter. Only 841 entries are 'resolved' sources ($\phi > 3$ mas), and 252 have no angular diameter estimate reported in the JSDC. The 5 'large' sources are: α Ori ($\phi \sim 45$ mas); α Sco ($\phi \sim 42$ mas); γ Cru ($\phi \sim 28$ mas); α Tau ($\phi \sim 23$ mas); and β Peg ($\phi \sim 20$ mas). Fig. 7 shows the all-sky coverage of these 841 sources. The size of the dots is proportional to ϕ.

4.6 MIR flux distribution

Fig. 8 shows the distributions in median flux for the L, M, and N bands:

(i) lower quartile flux: 0.07 Jy (L), 0.04 Jy (M), and 0.01 Jy (N);
(ii) median flux: 0.17 Jy (L), 0.09 Jy (M), and 0.02 Jy (N);
(iii) upper quartile flux: 0.6 Jy (L), 0.3 Jy (M), and 0.1 Jy (N).

About 36 per cent of the entries have $F_L < 0.1$ Jy (51 per cent for M, 78 per cent for N). Fig. 9 shows the distributions in flux dispersion for the L, M, and N bands. The mean ratio dispersion to flux value (relative dispersion, *rdisp*) is 6 per cent for the L and M bands, and 15 per cent for the N band:

(i) lower quartile relative dispersion: 2 per cent (L), 1 per cent (M), and 6 per cent (N);
(ii) median relative dispersion: 4 per cent (L), 2 per cent (M), and 10 per cent (N);
(iii) upper quartile relative dispersion: 8 per cent (L), 6 per cent (M), and 23 per cent (N).

We divide the sources contained in our catalogue according to their median flux F and correlated flux C in the L and N bands, assuming the UD model and the 130-m projected baselength. The relation between C and F is

$$C/F = V = 2\,\frac{|J_1(\pi\phi B/\lambda_c)|}{\pi\phi B/\lambda_c}, \quad (1)$$

where $B = 130$ m, $\lambda_c = 3.5$, 4.8, and 10.5 μm for the L, M, and N bands, respectively, and ϕ is the UD diameter for the considered band (reported in the JSDC). We define the four following subsets derived from the preliminary sensitivity performance of VLTI/MATISSE obtained during the commissioning phase, with corresponding ranges in flux and correlated flux given in Table 6:

(i) 'Bright' sources, for which the calibration quality in visibility is independent of the flux value.
(ii) 'Medium-bright' sources, for which the calibration quality in visibility depends on the flux value.
(iii) 'Faint' sources, which remain observable and useable for coherent flux observation.
(iv) 'Undetectable' sources, for which no fringe detection is achieved with current standard observations.

Table 7 gives the number of entries for each brightness subset, using the ATs and the UTs in the L and N bands. Figs 10 and 11 show the all-sky coverage of the 'UT-bright' sources for the L and N bands, respectively. In both figures, the size of the dots is proportional to the correlated flux in the considered band.

4.7 Flags distribution and 'pure' calibrators

Table 8 gives the truth table showing the possible values of CalFlag, with the number of entries corresponding to each value. Let us recall that CalFlag, reported in the JSDC (for detail see the description provided in the CDS/VizieR data base for the II/346 JSDC catalogue), is a 3-bit flag taking values ranging from '0' to '7':

(i) bit 1 is set if the chi-square associated with the reconstructed log diameter is > 5;
(ii) bit 2 is set if the star is a known double in WDS with separation <1 arcsec;
(iii) bit 3 is set if the star is, according to its SIMBAD's object type, a known spectroscopic binary, an Algol type star, a pulsating star, etc.

Downloaded from https://academic.oup.com/mnras/article/490/3/3158/5583026 by guest on 10 February 2023

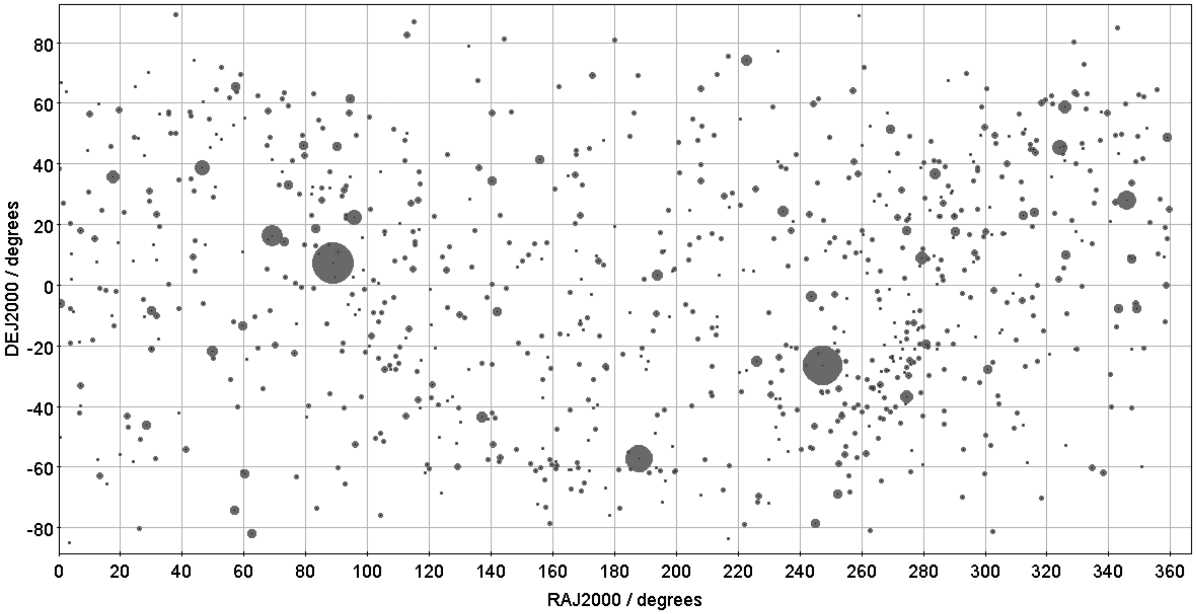

Figure 7. All-sky coverage of the 841 'resolved' sources contained in our catalogue ($\phi > 3$ mas). The size of the dots is proportional to the value of the LDD diameter reported in the JSDC.

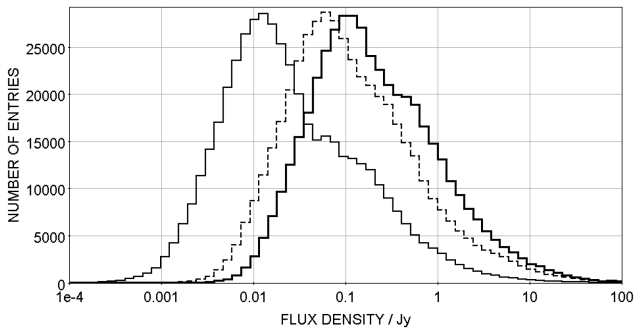

Figure 8. Distributions in flux density for the bands: *L* (thick solid line), *M* (thin dotted line), and *N* (thin solid line).

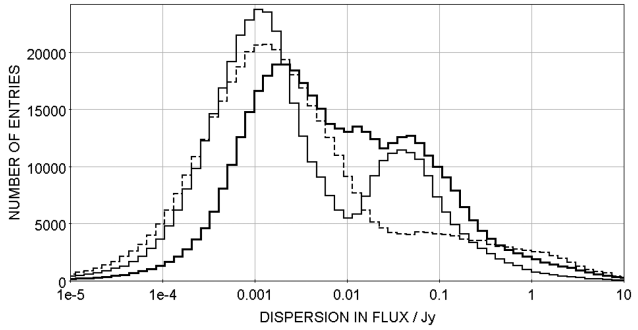

Figure 9. Distributions in flux density dispersion for the bands: *L* (thick solid line), *M* (thin dotted line), and *N* (thin solid line).

Although none of these flag values prevent the LDD diameter estimate to be accurate, they imply some caution in choosing this star as a calibrator star for OLBI.

Table 9 gives the truth table showing the possible values of IRflag, with the number of entries corresponding to each value. Let us recall that our new IRflag is also a 3-bit flag taking values ranging from '0' to '7':

(i) bit 1 is set if the star shows an IR excess, identified thanks to the [*K*-*W*4] and [*J*-*H*] colour indexes, and the overall MIR excess statistic X_{MIR} computed from *Gaia* DR1;
(ii) bit 2 is set if the star is extended in the IR, indicated by the extent flags reported in the *WISE*/AllWISE and AKARI catalogues;
(iii) bit 3 is set if the star is a likely variable in the MIR, identified by the variability flags reported in the *WISE*/AllWISE catalogues, the MSX6C Infrared Point Source Catalogue, the IRAS PSC, and the 10-micron Catalogue.

Table 10 gives the number of entries of the catalogue for each value of the pair (CalFlag;IRflag).

We consider those entries of the catalogue as MIR interferometric calibrators which:

(i) have a reliable angular diameter estimate;
(ii) are single stars or binaries with $\varepsilon > 1$ arcsec;
(iii) have a favourable Object Type;
(iv) show no IR-excess;
(v) show no IR-extent; and
(vi) is unlikely variable in the MIR.

We find 201 200 entries (43 per cent of the total number of entries of the catalogue) that satisfy these 6 conditions (i.e. with null CalFlag and IRflag). We consider them as 'pure' calibrators useable by high angular resolution instruments operating in the MIR. Strictly speaking, stars that do not fulfil this list of criteria should be kept with caution if used as interferometric calibrators. Finding stars fulfilling these criteria does not ensure them to be undoubted calibrators but potential ones only. For this reason, we strongly suggest to use more than one calibrator associated with each science target for the purpose of interferometric calibration.

Downloaded from https://academic.oup.com/mnras/article/490/3/3158/5583026 by guest on 10 February 2023

Table 6. Brightness subsets derived from the preliminary sensitivity performance of VLTI/MATISSE obtained during the commissioning phase. The values of flux F and correlated flux C in the L and N bands are in Jy.

	ATs				UTs			
Subset	F_L	C_L	F_N	C_N	F_L	C_L	F_N	C_N
Bright	–	>10	–	>90	–	>0.7	>5	>3
Medium bright	1.5–10	1–10	28–90	20–90	0.1–0.7	0.07–0.7	1.5–5	0.7–3
Faint	–	0.2–1	–	4–20	–	0.015–0.07	–	0.15–0.7
Undetectable	–	< 0.2	–	< 4	–	< 0.015	–	< 0.15

Table 7. Number of entries for each brightness class in the L and N bands, using the ATs and the UTs.

Subset	ATs		UTs	
	L	N	L	N
Bright	8 221	44	101 431	2 605
Medium bright	46 298	253	197 707	5 011
Faint	138 793	2 857	110 322	58 457
Undetectable	249 976	462 220	12 120	386 358

5 SELECTING CALIBRATORS FOR OBSERVATIONS WITH MATISSE

MATISSE is the second-generation spectro-interferometer of the VLTI, designed to observe in the L, M, and N bands. Preparing the commissioning and the science observations with MATISSE triggered the work described in this paper. MATISSE has several types of spectro-interferometric observables that can be used for model fitting and for image reconstruction. All these observables must be calibrated using a target for which their value is known, ideally a point source, or at least a disc with known diameter. This already excludes the binaries and the targets with IR excess that are unlikely to be well-defined discs. The other parameters of a calibrator, such as the flux, the coherent flux and the angular proximity with the science target have to be selected with different criteria for the different observables and for the observation spectral band. The ideal calibrator has the same flux and the same coherent flux in L and N and is observed through the same atmospheric conditions, which means that its angular distance with the science target is small (less than a few degrees) and the 'Cal-Sci' cycle is fast. In practice such a calibrator almost never exists. So, it might be necessary to use several calibrators to fulfil different constraints. In the following we try to propose criteria allowing the number of calibrators to be minimized and therefore the telescope time spent for the science target itself to be maximized.

The full calibration procedure of all MATISSE observables is a complex issue as there are several possible calibration strategies that can be adapted to the MATISSE observable favoured by the user. A full discussion is beyond the scope of this paper and we give here only some global indications to ease the choice of the relevant calibrators.

The first observable of MATISSE is the coherent flux in each spectral channel $C_{ij} = V_{ij}\ R_{ij}\ \sqrt{S_i\ S_j}$ where V_{ij} is the source visibility, R_{ij} is the instrumental response in visibility, and S_i is the contribution of beam i to the flux in the interferometric way. In the terminology of interferometric instruments S_i is called the 'photometry'. The photometry can be written as $S_i = T_i\ \eta_i\ F$, where T_i is the fixed and calibrated transmission of the instrument in the beam i, η_i is a time-variable coupling efficiency that depends on the atmosphere and instrument variations through the Strehl ratio and the image jitter, and F is the absolute flux of the source.

An estimate of the response in visibility is provided by the observation of a reference star (calibrator), assuming no change of the instrumental response between the observation of the science target and its calibrator. Thus the coherent flux of the science target in each spectral channel can be written as

$$C_{\mathrm{sci},ij} = V_{\mathrm{sci},ij}\, R_{ij} \sqrt{S_{\mathrm{sci},i}\, S_{\mathrm{sci},j}} = \frac{V_{\mathrm{sci},ij}}{V_{\mathrm{cal},ij}} C_{\mathrm{cal},ij} \sqrt{\frac{S_{\mathrm{sci},i}\, S_{\mathrm{sci},j}}{S_{\mathrm{cal},i}\, S_{\mathrm{cal},j}}}, \qquad (2)$$

where the $_{\mathrm{sci}}$ subscript stands for the science target, and $_{\mathrm{cal}}$ for the calibrator.

5.1 Absolute visibility

The most usual interferometric observable is the absolute visibility in each spectral channel, defined according to equation (2) as

$$V_{\mathrm{sci},ij} = \frac{C_{\mathrm{sci},ij}}{C_{\mathrm{cal},ij}}\ V_{\mathrm{cal},ij} \sqrt{\frac{S_{\mathrm{cal},i}\ S_{\mathrm{cal},j}}{S_{\mathrm{sci},i}\ S_{\mathrm{sci},j}}}. \qquad (3)$$

Computing the ratio $(S_{\mathrm{cal},i}\ S_{\mathrm{cal},j})$ / $(S_{\mathrm{sci},i}\ S_{\mathrm{sci},j})$ is the goal of the photometric calibration of MATISSE. The photometric measures S_i are deduced by MATISSE itself using different parts of the detector or immediately after the interferometric measures. In both cases we introduce photometric errors that can bias the absolute visibility. To minimize this bias, one must use a photometric calibrator with the same flux as the science target, with a relative difference compatible with the error budget on the visibility. A difference of flux between the science and the photometry target of x per cent will introduce a relative error of the same x per cent on the visibility estimated using equation (3). An alternative way is to use a bright photometric calibrator to estimate the photometric bias that is currently of about 0.2 Jy in L and 5 Jy in N with the ATs. This requires calibrators brighter than 1.5 Jy in L and 50 Jy in N for 10 per cent-accuracy estimates. The photometric calibrator does not need to have a well-defined spatial structure but its flux and spectrum within the field of MATISSE must be known with the above accuracy. We see that the photometric calibration is a major issue in N.

5.2 Differential visibility and coherent flux ratio

MATISSE can use many observables that are not sensitive to photometric calibration errors, such as:

(i) the differential visibility in each spectral channel V_{ij} / $\overline{V}_{ij(\lambda)}$, where $\overline{V}_{ij(\lambda)}$ is the average visibility over the spectral bandwidth excluding the reference spectral channel;

(ii) the coherent flux ratio in each spectral channel C_{ij} / $C_{\mathrm{B_{min}}}$, where all baselines are calibrated by (for example) the shortest one B_{min}.

These measurements still need a calibration of the instrumental response in visibility R_{ij}. The relevant interferometric calibrator

Downloaded from https://academic.oup.com/mnras/article/490/3/3158/5583026 by guest on 10 February 2023

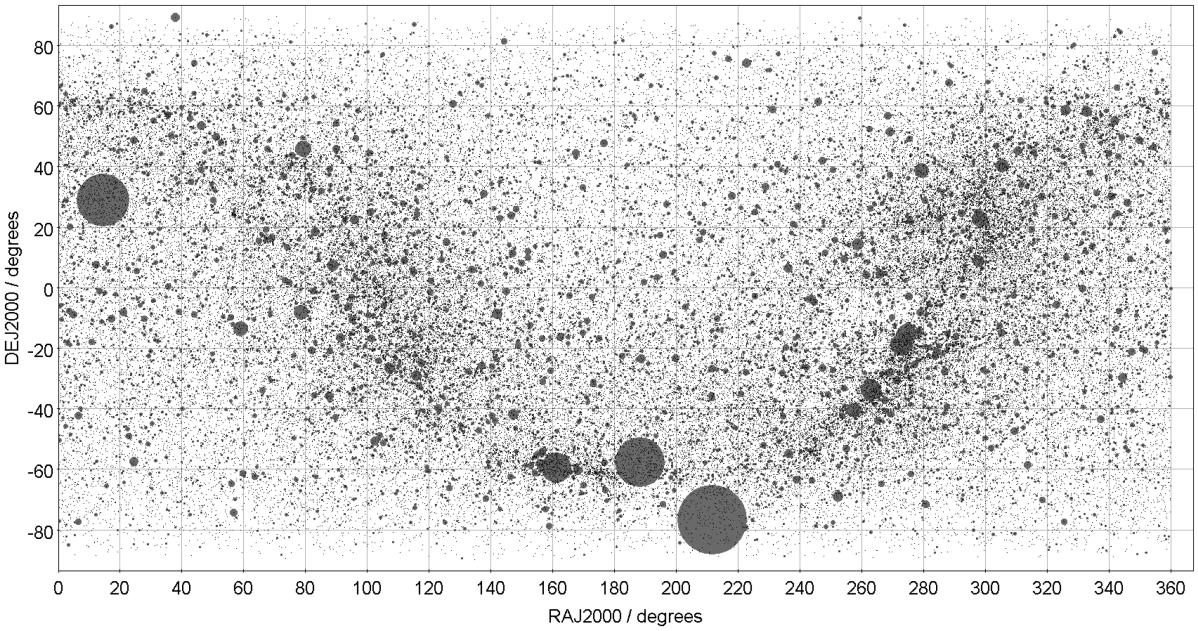

Figure 10. All-sky coverage of the 101 431 'UT-bright' sources for the L band ($C_L > 0.7$ Jy). The size of the dots is proportional to C_L.

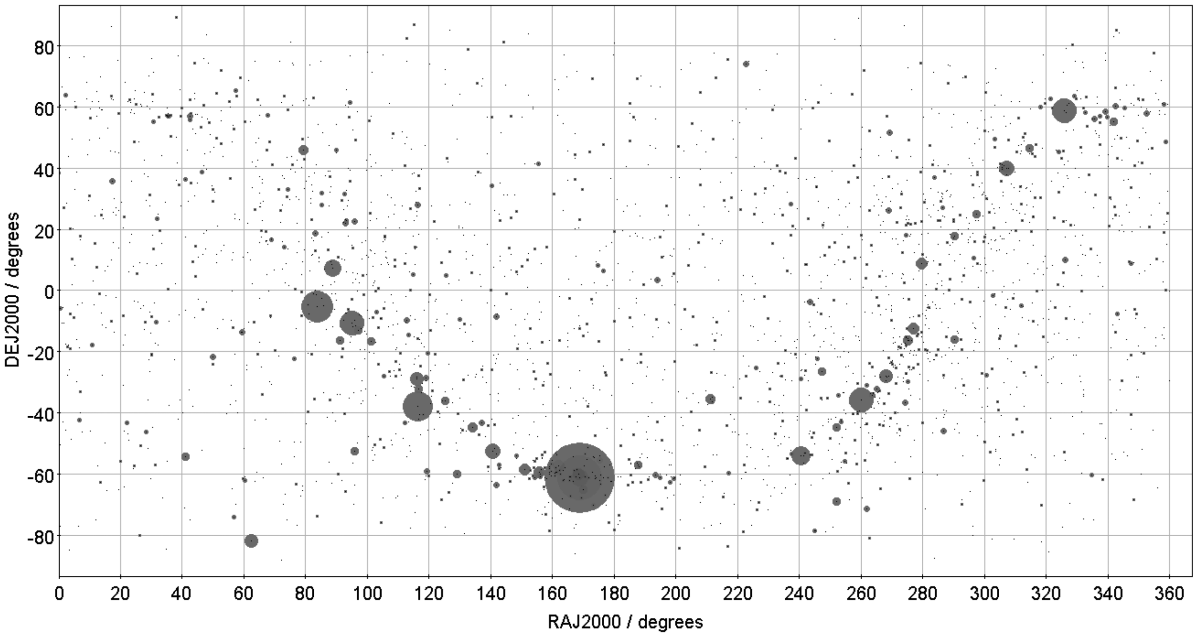

Figure 11. All-sky coverage of the 2 605 'UT-bright' sources for the N band ($F_N > 5$ Jy and $C_N > 3$ Jy). The size of the dots is proportional to C_N.

must be a point source or a disc with an accurate diameter. It must be brighter than the science target. In the L band, R_{ij} is quite sensitive to the seeing conditions and mainly to the coherence time τ_0. It is therefore important to observe it as close as possible in space and time to the science target. For accurate instrument visibility calibration, it is recommended to use a 'Cal1-Sci-Cal2' sequence with an average airmass for the 2 calibrators identical within 3 per cent to that of the science target. For coherent fluxes larger than about 10 Jy in L and 90 Jy in N with ATs, the contribution of fundamental noise becomes small with regard to the other contributions. In the N band, R_{ij} is much less sensitive to atmospheric variations, and the calibrator should be brighter than the science target, without companion and infrared excess, regardless of its proximity to the science target.

5.3 Differential phase

The differential phase in each spectral channel $\phi_{ij} - \overline{\phi}_{ij(\lambda)}$ (with the same definition of the reference channel than for the differential visibility), representing the change of phase with wavelength, is sensitive only to instrument artefacts (mostly detector features) and the chromatic optical path difference (OPD) introduced by the atmosphere and the difference of airpath in the delay line tunnels. The detector features are in principle calibrated by an internal

Downloaded from https://academic.oup.com/mnras/article/490/3/3158/5583026 by guest on 10 February 2023

Table 8. Truth table of CalFlag and number of entries. OType is the Object Type in SIMBAD.

CalFlag	$\chi^2 > 5$	$\varepsilon < 1$ arcsec	Bad OType	# of entries
'0'	No	No	No	450 921
'1'	Yes	No	No	371
'2'	No	Yes	No	8090
'3'	Yes	Yes	No	31
'4'	No	No	Yes	5965
'5'	Yes	No	Yes	66
'6'	No	Yes	Yes	404
'7'	Yes	Yes	Yes	9

Table 9. Truth table of IRflag and number of entries for each value of the flag.

IRflag	IR-excess	IR-extent	MIR-var.	# of entries
'0'	No	No	No	207 434
'1'	Yes	No	No	162 899
'2'	No	Yes	No	30 570
'3'	Yes	Yes	No	36 020
'4'	No	No	Yes[a]	4815
'5'	Yes	No	Yes[a]	4345
'6'	No	Yes	Yes[a]	7075
'7'	Yes	Yes	Yes[a]	12 699

Note. [a]The MIR variability is defined in Section 3.3. The likely variable sources must fulfil at least one of the following criteria: (i) variability flag > 6 in at least one of the *WISE* filters *W*1, *W*2, or *W*3; (ii) variability flag = 1 in at least one of the MSX filters *B*1, *B*2, *C*, or *A*; (iii) likelihood of variability >90 per cent IRAS/12 filter; (iv) tagged as variable in the 10-micron Catalogue.

Table 10. Crossed distribution of CalFlag and IRflag.

IR-flag	CalFlag '0'	'1'	'2'	'3'	'4'	'5'	'6'	'7'
'0'	201 200	16	4034	0	2019	0	165	0
'1'	158 992	146	2431	6	1269	11	44	0
'2'	29 412	21	584	1	483	2	64	3
'3'	34 875	75	541	9	462	20	35	3
'4'	4434	3	95	0	271	0	12	0
'5'	3752	23	76	1	482	6	5	0
'6'	6495	32	141	5	340	6	54	2
'7'	11 761	55	188	9	639	21	25	1

MATISSE calibration. At this point, we do not have a reliable and accurate model for the chromatic OPD and it is recommended to calibrate the differential phase with calibrators introducing the same air path difference, i.e. at the same declination and with hour angles allowing them to be observed in the same position on the sky than the science target, with calibrators brighter than their science target.

5.4 Closure phase

The closure phase in each spectral channel $\psi_{ijk} = \phi_{ij} + \phi_{jk} + \phi_{ki}$ is in principle self-calibrated by MATISSE, but it remains sensitive to fast detector variations and it can be slightly contaminated by the chromatic OPD that affects the differential phase, for example because of crosstalk between MATISSE beams or fringe peaks. It is therefore recommended to calibrate it with the same calibrators as for the differential phase.

5.5 Imaging runs

During imaging runs, many observations of a science target are repeated. They should be merged with calibrators fulfilling all the conditions above:

(i) Cal1L and Cal2L for instrument and atmosphere calibration in the *L* band. At least one of them should be chosen to be also a good chromatic OPD calibrator.
(ii) CalPL for a photometric calibration in the *L* band.
(iii) CalPN for photometric calibration in the *N* band.
(iv) Cal3N for interferometric calibration in the *N* and.

The photometric calibrator can be used only once per sequence, while the interferometric ones must be repeated regularly. Of course, one should try to reduce the number of calibrators choosing for instance Cal2L = CalPL and Cal3N = CalPN.

6 THE PRIMARY LISTS OF CALIBRATOR CANDIDATES FOR VLTI/MATISSE

6.1 Requirements

From our catalogue, we extract lists of calibrator candidates for the *L* and *N* bands, based on their angular diameter, object type, degree of binarity, infrared brightness and features. The selected targets are bright point-like stars observable with the VLTI/MATISSE. Since our goal is to provide a self-consistent interferometric network of calibrators suitable for VLTI/MATISSE, we have started a large observing programme in order to measure their angular diameter with high accuracy (1 per cent or even better) in the MIR spectral bands.

6.2 Selection criteria

The candidate calibration stars must satisfy the following conditions, listed in the order they are applied to the building process of our catalogue:

(i) The source must be observable from the ESO-Paranal Observatory (latitude 24° 40' S). This condition provides a subset of 371 333 candidates.
(ii) The source must be a potential calibrator suitable for optical long-baseline interferometry (CalFlag of '0'). This flag condition provides a subset of 359 580 calibrator candidates observable from Paranal.
(iii) The source must be as small as possible in order to minimize the calibration error caused by the uncertainty in the calibrator modelling. Fig. 12 shows the distribution of the relative error in the LDD diameter given by the JSDC for the 'pure' (IRflag of '0') and excess-free (IRflag of '0', '2', '4', or '6') calibrators. The mean value of the relative error in angular diameter is about 2.6–2.7 per cent. Using the UD model, one can demonstrate (see e.g. Bordé et al. 2002) that the relative error in visibility $\Delta V/V$ remains lower than the relative error in angular diameter $\Delta\phi/\phi$ provided that $\phi < 0.59\ \lambda/B$ (corresponding to $V > 0.63$), as shown in Fig. 13. For the 130-m projected baselength this condition corresponds to $\phi < 3.3$ mas for $\lambda = 3.5$ μm, and $\phi < 10$ mas for $\lambda = 10.5$ μm. Choosing targets with $\phi < 3$ mas for the *L* band or $\phi < 9$ mas for the *N* band ensures that $\Delta V/V < 0.8\ \Delta\phi/\phi$, in both bands for any baseline smaller than 130 m ($\phi\ B/\lambda < 0.54$; $V > 0.68$). With this size condition, 15 sources are excluded from the subset for the *N* band, while 542 sources are excluded for the *L* band.

Downloaded from https://academic.oup.com/mnras/article/490/3/3158/5583026 by guest on 10 February 2023

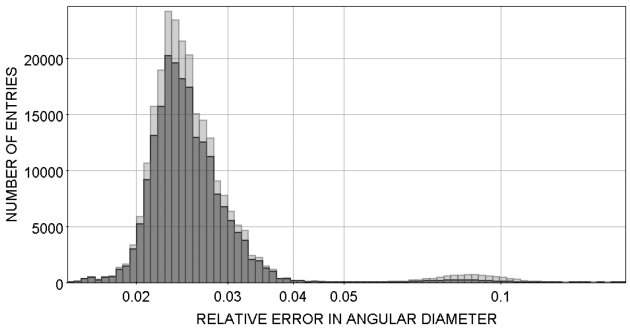

Figure 12. Distribution of the relative error in the LDD diameter reported in the JSDC for the 'pure' (dark grey) and excess-free (grey) calibrators.

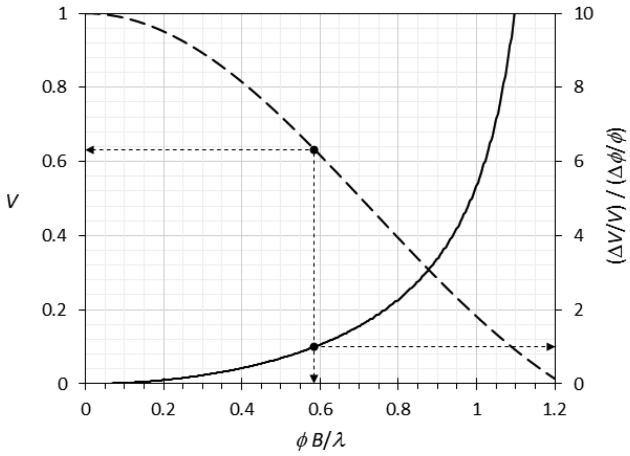

Figure 13. Ratio of the relative error in UD visibility to the relative error in angular diameter (solid line, right scale), and UD visibility (dashed line, left scale), versus the angular diameter in angular resolution unit. The black dots are the points of the 2 curves of same abscissa $\phi\, B/\lambda \sim 0.59$ (corresponding to $\Delta V/V = \Delta\phi/\phi$).

(iv) To ensure a good confidence level in the final flux estimate, we exclude the sources with a large dispersion of the photometric points and those with less than 2 photometric points. Since 90 per cent of the entries of our catalogue have *rdisp* < 0.14 in *L* or *rdisp* < 0.29 in *N* (*rdisp* is the relative dispersion, given by the ratio of the dispersion to the flux value), we exclude the sources with *rdisp* > 0.15 in *L* and *rdisp* > 0.3 in *N*. Observing with the VLTI/MATISSE on all four UTs is a rather expensive undertaking and it is therefore important to reduce the on-sky calibration time as much as possible. Therefore we also look for calibrators that are both compact enough to serve as *L*-band calibrators ($\phi < 3$ mas), while still being bright enough in the *N* band to also serve as *N*-band calibrators. We call them 'hybrid' calibrators. Using the ATs, 304 816 candidates are kept for *L*, 307 815 candidates for *N*, and 285 688 are hybrid calibrators.

(v) The sources must be detectable with MATISSE and useable at least for coherent flux measurements. Thus, they must belong to the category of 'faint' sources or even brighter, as defined in Table 6:

(a) With ATs, this corresponds to $C_L > 0.2$ Jy and $C_N > 20$ Jy. We find 142 620 potential candidates suitable for *L*, 1642 for *N*, and 656 for both bands (hybrid).

(b) With UTs, this corresponds to $C_L > 0.015$ Jy and $C_N > 0.15$ Jy. We find 300 332 potential candidates suitable for *L*, 49 345 for *N*, and 40 077 for both bands (hybrid).

6.3 Results

Table 11 gives the final numbers of *L* band, *N* band, and hybrid candidates suitable with the ATs and the UTs, for each subset of brightness limit (bright targets, 'med+' = bright + medium-bright targets, 'faint+' = bright+medium-bright+faint targets), and for different values of IRflag.

We find only 1 hybrid bright 'pure' calibrator candidate suitable for the ATs (V343 Pup), and 14 'pure' calibrator candidates suitable for the UTs. To explain the small numbers of hybrid 'pure' calibrators, we invoke the fact that the 'standard' stars, i.e. showing no IR-excess, have their flux density in *L* always higher than in *N*. The statistics of the flux ratio *L* to *N* for the 'pure' calibrators is:

(i) lower quartile ratio F_L/F_N: 7;
(ii) median ratio: 8.4;
(iii) upper quartile ratio: 9.

Fig. 14 shows that the distribution of the flux ratio for the 'pure' calibrators reveals 2 peaks around the values of 7 and 9. If we compute the flux ratio at $\lambda = 3.5$ μm to the flux at $\lambda = 10.5$ μm for the same stars assumed to be blackbodies, we find that the distribution of the flux ratio shows a single peak around 7 (dashed overplotted histogram of Fig. 14). We suspect the second peak of the flux ratio distribution (around 9) to be caused by stars with SEDs deviating from simple blackbodies, showing sort of 'infrared deficits' probably caused by the presence of absorption bands in this spectral domain.

As primary lists of calibrator candidates, we select the lists of excess-free candidates (IRFlag of '0', '2', '4', or '6'): hybrid-bright for the UTs (259 entries); *L*-bright (1 621 entries), *N*-'med+' (44 entries), and hybrid-'faint+' (375 entries) for the ATs. We note that all the 259 hybrid UT-bright candidates are *L* band AT-bright candidates, and are hybrid AT-'faint+' candidates as well. All the 375 hybrid AT-'faint+' candidates are also *L* band AT-bright candidates.

Matching our primary lists with the MIDI and the Cohen lists formerly used for MIR interferometry, we find 95 *L* band AT-bright candidates that are MIDI calibrators and 127 that are Cohen's standards; 22 *N* band AT-'med+' candidates that are MIDI calibrators and 18 that are Cohen's standards; 79 hybrid AT-'faint+' candidates that are MIDI calibrators and 113 that are Cohen's standards; 79 hybrid UT-bright candidates that are MIDI calibrators and 103 that are Cohen's standards. A detailed analysis of the original MIDI and Cohen's lists reveals that only 10 MIDI calibrators and 15 Cohen's standards are 'pure' calibrators (with null CalFlag and IRflag), which may suggest that our flag criteria to identify the 'pure' calibrators are much more selective than the criteria used to build the MIDI and the Cohen's lists. Relaxing the IRflag constraint, we find that 244 MIDI calibrators (among 402) and 291 Cohen's standards (among 422) are excess-free calibrators (with null CalFlag and IRflag of '0', '2', '4', or '6').

Table 12 reports the first 10 rows of the list of the 375 hybrid AT-'faint+' excess-free calibrator candidates, ordered by their increasing right ascension. For brevity, we give the name of each selected source, with its spectral type, coordinates (J2000), angular diameter values with associated errors reported in the MIDI list, the Cohen's list, and the JSDC, flux and correlated flux values with errors in the *L* and *N* bands. To get a rough estimate of the relative

Downloaded from https://academic.oup.com/mnras/article/490/3/3158/5583026 by guest on 10 February 2023

Table 11. Number of entries for each brightness-limit subset of calibrator candidates suitable with ATs and UTs in the *L* and *N* bands for different values of IRflag. 'Hybrid' calibrators are for both bands. 'Med+' stands for 'Medium-bright+bright' and 'Faint+' stands for 'Faint+Medium-bright+bright'. The 'bright', 'medium-bright', and 'faint' categories are defined in Table 6. The 4 numbers in bold are those of the 4 final primary lists of excess-free calibrator candidates.

		ATs			UTs		
Subset	IRflag	*L*	*N*	Hybrid	*L*	*N*	Hybrid
Bright	'0' to '7'	2851	17	1	61 500	1295	455
	'0', '2', '4', or '6'	**1621**	3	0	56 068	581	**259**
	'0'	171	0	0	41 269	28	14
Med+	'0' to '7'	29 991	142	3	201 468	5293	2621
	'0', '2', '4', or '6'	26 314	**44**	0	158 715	2412	1476
	'0'	16 886	1	0	132 861	237	156
Faint+	'0' to '7'	142 620	1 642	656	300 332	49 345	40 077
	'0', '2', '4', or '6'	122 958	750	**375**	171 663	41 288	36 116
	'0'	101 295	40	22	144 113	27 751	24 828

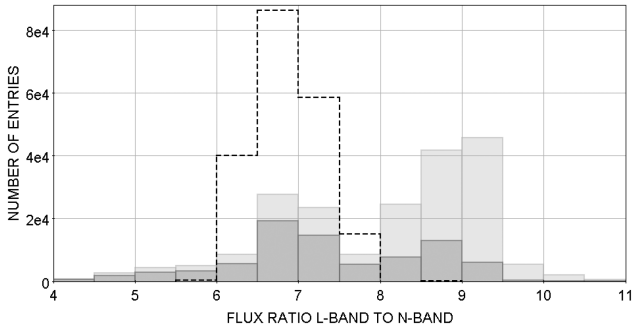

Figure 14. Distribution of the ratio of the flux density in *L* to *N* for the 'pure' calibrators (light grey: all spectral types; dark grey: late-type stars). The dashed histogram corresponds to the flux ratio *L* to *N* for the pure calibrators of all spectral types assumed to be blackbodies.

uncertainty in correlated flux, we simply add the relative uncertainty in angular diameter to the relative dispersion in flux. The value of IRflag is also reported in the list. The full table (containing the 375 entries) is available online.

6.4 Statistics of the primary lists

Figs 15–18, respectively, show the sky coverage of the *L* band AT-bright, *N* band AT-'med+', hybrid AT-'faint+', and hybrid UT-bright excess-free calibrator candidates. In each figure, the size of the dots is proportional to the 130-m UD correlated flux: in the *L* band for Fig. 15, in the *N* band for the three other figures.

From our study, we conclude that:

(i) Finding bright calibrators closer than a few degrees to any scientific target is not an issue for the *L* band, with both the UTs and the ATs.

(ii) With UTs, finding bright excess-free calibrator candidates suitable for both the *L* and the *N* bands (hybrid) is guaranteed in a circle of about 10–15° around any scientific target.

(iii) With ATs, no source of the catalogue can be used as a bright calibrator candidate suitable for both bands. To find an hybrid calibrator in a circle of 10° around any scientific target, we need to include the medium-bright and the faint sources ('faint+').

(iv) With ATs in the *N* band, our catalogue gives only 3 bright and 44 bright+medium-bright ('med+') excess-free calibrator candidates observable with the VLTI/MATISSE. Unless including the faint sources as well, the average distance from target to 'med+' excess-free calibrator is rarely less than 20–25°.

Fig. 19 shows the distribution in spectral and luminosity classes of the calibrators for each list. We count 1 290 K-giants (with luminosity class III) in the *L* band AT-bright list; 34 in the *N* band AT-'med+' list; 316 in the hybrid AT-'faint+' list; and 221 in the hybrid UT-bright list.

Fig. 20 shows the distribution of the relative error in angular diameter reported in the JSDC for the *L* band AT-bright and the hybrid AT-'faint+' excess-free calibrator candidates. The mean relative error in angular diameter is 10 per cent for the *N* band AT-'med+' excess-free calibrator candidates and 9 per cent for the excess-free calibrator candidates of the three other lists. These values are significantly higher than the mean value of 2.6 per cent obtained with the complete initial set of calibrator candidates (see Fig. 12). As shown in Fig. 13, to obtain visibility measurement within 1 per cent accuracy, a calibration error of 10 per cent level needs the use of UD calibrators with $\phi < 1.1$ mas for the *L* band, and $\phi < 3.3$ mas for the *N* band with the 130-m baselength ($\phi\ B/\lambda < 0.2$; $V_{\rm ud} > 0.95$).

Since Chelli et al. (2016) claimed that the method they used to estimate the angular diameter reported in the JSDC (derived from the surface brightness method) does not depend on the luminosity class, we invoke the spectral class only to explain this discrepancy in diameter uncertainty. In our lists, the K and M stars represent 83 per cent of the *L* band AT-bright, 91 per cent of the *N* band AT-'med+', and 87 per cent of both the AT-'faint+' and the UT-bright hybrid excess-free calibrator candidates, while they represent only 40 per cent of the total set of excess-free calibrator candidates in our catalog. The high level of diameter uncertainty (9–10 per cent) reported in the JSDC for our calibrator candidates confirms the crucial need for measuring the angular diameter of the calibrators for the VLTI/MATISSE (mainly giant stars) with 1 per cent accuracy (or even better).

Downloaded from https://academic.oup.com/mnras/article/490/3/3158/5583026 by guest on 10 February 2023

Table 12. Sample table showing the first 10 hybrid AT-'faint+' excess-free calibrator candidates, ordered by their increasing right ascension. $\phi_{\rm MIDI}$, $\phi_{\rm Cohen}$, and $\phi_{\rm JSDC}$ are the angular diameter estimates, respectively, reported in the MIDI list, the Cohen's list, and the JSDC. $\Delta\phi_{\rm MIDI}$, $\Delta\phi_{\rm Cohen}$, and $\Delta\phi_{\rm JSDC}$ are their associated uncertainties. F_L and F_N are the flux density in bands L and N, respectively. ΔF_L and ΔF_N are their associated uncertainties. C_L and C_N are the correlated flux for the UD model with the 130-m baselength in the L and N bands, respectively. ΔC_L and ΔC_N are their associated uncertainties. The full table (containing the 375 entries) is available online.

Name	Spectral Type	αJ2000 (h:m:s)	δJ2000 (d:m:s)	$\phi_{\rm MIDI}$ (mas)	$\Delta\phi_{\rm MIDI}$ (mas)	$\phi_{\rm Cohen}$ (mas)	$\Delta\phi_{\rm Cohen}$ (mas)	$\phi_{\rm JSDC}$ (mas)	$\Delta\phi_{\rm JSDC}$ (mas)	IRflag	F_L (Jy)	ΔF_L (Jy)	F_N (Jy)	ΔF_N (Jy)	C_L (Jy)	ΔC_L (Jy)	C_N (Jy)	ΔC_N (Jy)
kap02 Scl	K2III	00:11:34.419	−27:47:59.03	–	–	1.73	0.03	1.72	0.15	2	34.7	4.7	5.6	1.4	30.9	7.0	5.6	1.8
HD 853	M2III	00:12:55.139	−03:22:53.56	–	–	–	–	2.25	0.16	6	18.4	1.9	5.0	1.2	15.0	2.7	4.9	1.5
HD 942	K5III	00:13:42.245	−26:01:20.44	–	–	–	–	2.26	0.19	6	43.1	4.8	6.9	0.9	35.1	6.9	6.8	1.5
HD 1063	M0III	00:14:55.762	−03:01:38.69	–	–	–	–	1.97	0.16	6	24.0	1.5	4.3	1.2	20.6	3.0	4.2	1.6
HD 1187	K2III	00:16:08.867	−31:26:47.02	–	–	–	–	1.56	0.15	6	27.0	1.0	4.1	1.0	24.5	3.3	4.0	1.4
HD 1923	M2III	00:23:22.145	−29:50:50.11	–	–	–	–	2.42	0.19	0	39.0	2.5	5.6	1.3	30.7	4.4	5.5	1.7
eps And	G7III	00:38:33.346	+29:18:42.31	–	–	–	–	1.86	0.16	6	40.2	1.9	6.4	1.5	35.0	4.6	6.3	2.0
mu Phe	G8III	00:41:19.552	−46:05:06.02	–	–	–	–	1.75	0.15	6	32.6	2.9	5.2	0.4	28.9	5.0	5.2	0.8
Cl Psc	M3III	00:44:55.279	+03:12:03.59	–	–	–	–	2.30	0.21	2	32.7	1.8	5.7	1.7	26.3	3.8	5.6	2.2
HD 5098	K1III	00:52:40.625	−24:00:21.04	–	–	–	–	1.60	0.16	6	28.5	0.2	4.5	1.1	25.7	2.7	4.4	1.5
...																		

7 CONCLUSIONS

We have built a new all-sky catalogue, called the Mid-infrared stellar Diameter and Flux compilation Catalogue (MDFC), that contains 465 857 entries with the aim of helping the users of long-baseline interferometers operating in the mid-infrared with the preparation of their observations and the calibration of their measurements. The main improvement to the other existing catalogues is the specific extension to the mid-infrared wavelengths. Our catalogue covers the entire sky and contains mainly dwarf and giant stars from A to K spectral types, closer than 6 kpc. The smallest values of the reported median value in flux density are 0.16 mJy in the L band and 0.1 mJy in the N band. The smallest values of the reported diameter reach 1 microarcsec. The construction of the catalogue is divided in three main steps:

(i) The angular diameter estimates reported in the JSDC are complemented by the measurements compiled in the JMDC, the diameter estimates computed from the distance and the radius reported in the *Gaia* DR2 data release, and the diameter estimates reported in the VLTI/MIDI list of calibrator candidates and in the Cohen's list of spectrophotometric standards.

(ii) The median flux density and an estimate of the statistical dispersion in the L, M, and N bands are computed from the compilation of almost 20 photometric catalogues.

(iii) The information about the presence of circumstellar features around each source revealed by the IR data (excess, extent, and variability) is synthetized into a single 3-bit flag.

Our infrared flag, which is used complementary to the calibrator flag reported in the JSDC, allows us to report a list of 201 200 'pure' calibrators suitable for the mid-infrared. These sources are single stars or wide binaries with a favourable object type, have a reliable angular diameter estimate, and show no evidence for IR feature (excess, extent, variability).

Selecting only the excess-free calibrators, we produce the four primary lists of VLTI/MATISSE calibrators containing more than one thousand of them (mainly cool giants): with ATs for the L band (1621 bright sources), for the N band (44 bright and medium-bright sources), and for both bands (375 hybrid bright, medium-bright, and faint sources); with UTs for both bands (259 hybrid bright sources). They are selected according to:

(i) their declination;
(ii) the reliability and value of their angular diameter estimate;
(iii) their astrometric binarity;
(iv) their SIMBAD Object Type;
(v) the reliability and value of their MIR flux and correlated flux estimates; and
(vi) their IR excess.

Since they have not yet been measured or modelled with a better accuracy than 5 per cent, we have initiated a large observing programme with the VLTI/MATISSE in the aim to measure their angular diameter at 1 per cent accuracy. To get this challenging accuracy without any need of external calibration, we have developed a new method that will be the subject of a forthcoming paper.

ACKNOWLEDGEMENTS

This work uses the VizieR catalogue access tool, CDS, Strasbourg, France; the SIMBAD data base, operated at CDS, Strasbourg, France; and the TOPCAT software, provided by Mark Taylor of

Downloaded from https://academic.oup.com/mnras/article/490/3/3158/5583026 by guest on 10 February 2023

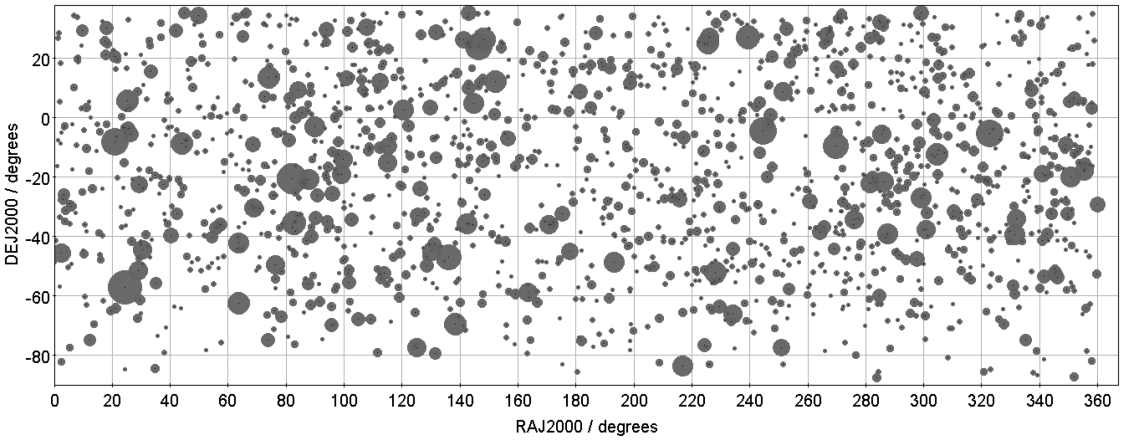

Figure 15. Sky coverage of the 1621 *L* band AT-bright excess-free calibrator candidates. The size of the dots is proportional to C_L.

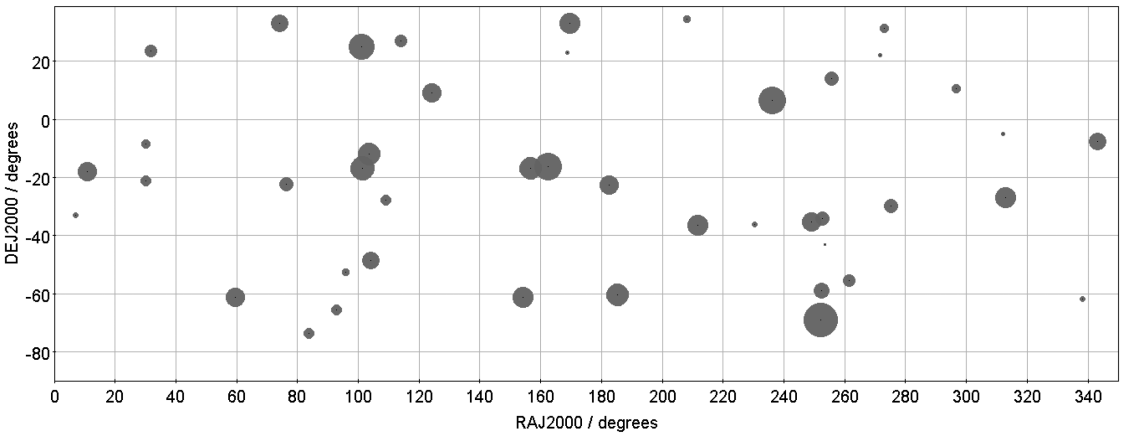

Figure 16. Sky coverage of the 44 *N* band AT-'med+' calibrator candidates. The size of the dots is proportional to C_N.

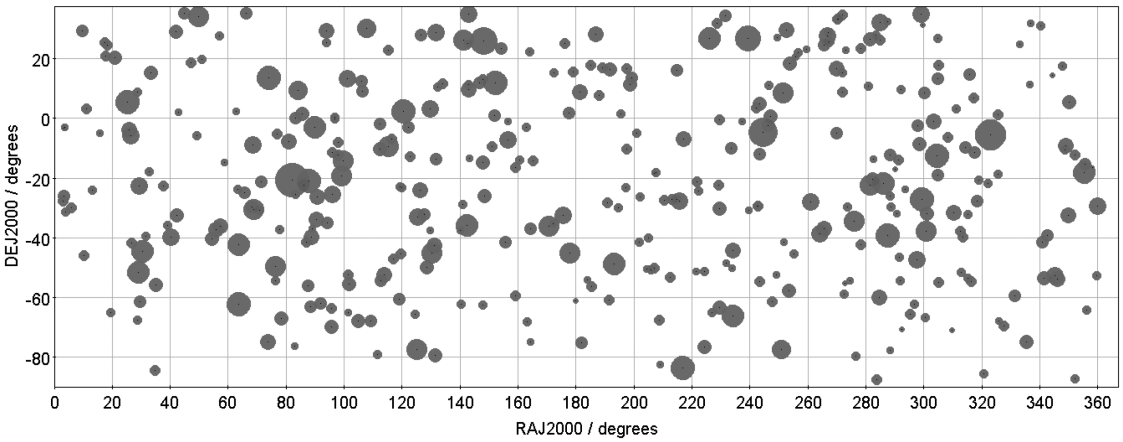

Figure 17. Sky coverage of the 375 hybrid AT-'faint+' calibrator candidates. The size of the dots is proportional to C_N.

Bristol University, England available at starlink.ac.uk/topcat. This publication makes use of the data products from:

(i) The *Hipparcos* and Tycho Catalogues;
(ii) The Tycho-2 Catalogue;
(iii) The *Gaia* data release 2 (DR2), *Gaia* team;
(iv) The Estimating distances from *Gaia* DR2 parallaxes catalog, Coryn Bailer-Jones calj@mpia.de;
(v) The *UBVRIJKLMNH* Photoelectric Photometric Catalogue;
(vi) The Catalogue of 10-micron celestial objects;
(vii) The *IRAS* Catalogue of Point Sources, Version 2.0, Joint *IRAS* Science W.G.;
(viii) The *IRAS* Faint Source Catalog, |b| > 10, Version 2.0;
(ix) The Two Micron All-Sky Survey, which is a joint project of the University of Massachusetts and the Infrared Processing and

Downloaded from https://academic.oup.com/mnras/article/490/3/3158/5583026 by guest on 10 February 2023

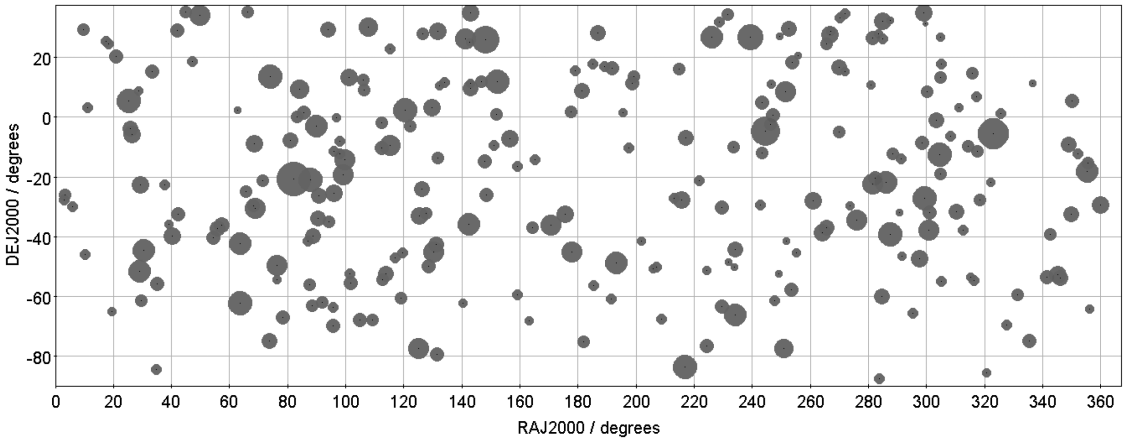

Figure 18. Sky coverage of the 259 hybrid UT-bright excess-free calibrator candidates. The size of the dots is proportional to C_N.

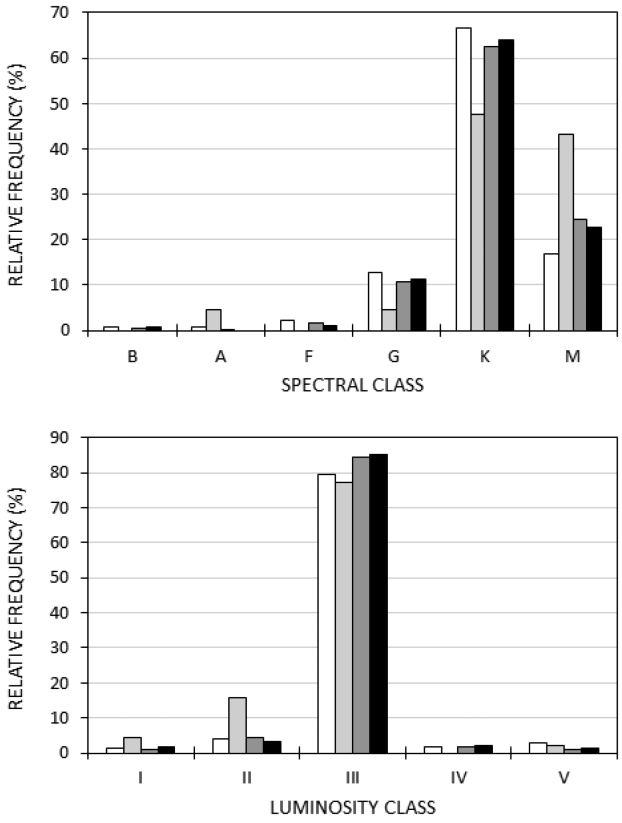

Figure 19. Distribution in spectral (top) and luminosity (bottom) class of the *L* band AT-bright (white), *N* band AT-'med+' (light grey), hybrid AT-'faint+' (dark grey), and hybrid UT-bright (black) excess-free calibrator candidates.

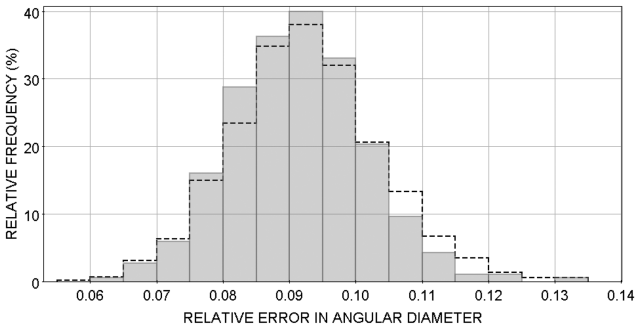

Figure 20. Distribution of the relative error in angular diameter reported in the JSDC for the 1621 *L* band AT-bright (black thin dashed steps) and the 375 hybrid AT-'faint+' (light grey filled bars) excess-free calibrator candidates.

Analysis Center/California Institute of Technology, funded by the National Aeronautics and Space Administration and the National Science Foundation;

(x) The Galactic Legacy Infrared Mid-Plane Survey Extraordinaire (GLIMPSE), Spitzer Science Center;

(xi) The AKARI/IRC Mid-Infrared All-Sky Survey (Version 1);

(xii) The Wide-field Infrared Survey Explorer, which is a joint project of the University of California, Los Angeles, and the Jet Propulsion Laboratory/California Institute of Technology, funded by the National Aeronautics and Space Administration, Roc Cutri (IPAC/Caltech);

(xiii) The *IRAS* PSC/FSC Combined Catalogue;

(xiv) The JMDC: JMMC Measured Stellar Diameters Catalogue, Gilles Duvert gilles.duvert@univ-grenoble-alpes.fr;

(xv) The Jean-Marie Mariotti Center JSDC catalogue, downloadable at http://www.jmmc.fr/jsdc, Gilles Duvert gilles.duvert@univ-grenoble-alpes.fr;

(xvi) The MSX6C Infrared Point Source Catalog;

(xvii) The Washington Double Star Catalogue maintained at the U.S. Naval Observatory;

(xviii) The *COBE* DIRBE Point Source Catalog, Beverly J. Smith beverly@nebula.etsu.edu;

(xix) The Parameters and IR excesses of Gaia DR1 stars catalogue, Iain McDonald iain.mcdonald-2@manchester.ac.uk;

(xx) The Stars with calibrated spectral templates list, downloadable at http://www.gemini.edu/sciops/instruments/mir/Cohen_list.html;

(xxi) The VLTI/MIDI calibrator candidates list, downloadable at http://ster.kuleuven.be/~tijl/MIDI_calibration/mcc.txt.

P. C. wants to thank A. Chiavassa, O. Creevey, D. Mourard, N. Nardetto, M. Schultheis, and F. Thévenin for their helpful comments and advice.

Downloaded from https://academic.oup.com/mnras/article/490/3/3158/5583026 by guest on 10 February 2023

REFERENCES

Abrahamyan H. V., Mickaelian A. M., Knyazyan A. V., 2015, Astron. Comput., 10, 99

Allouche F. et al., 2016, in Malbet F., Creech-Eakman M. J., Tuthill P. G., eds, Proc. SPIE Conf. Ser. Vol. 9907, Optical and Infrared Interferometry and Imaging V. SPIE, Bellingham, p. 99070C

Andrae R. et al., 2018, A&A, 616, A8

Bailer-Jones C. A. L., Rybizki J., Fouesneau M., Mantelet G., Andrae R., 2018, AJ, 156, 58

Benjamin R. A. et al., 2003, PASP, 115, 953

Bordé P., Coudé du Foresto V., Chagnon G., Perrin G., 2002, A&A, 393, 183

Bourgès L., Mella G., Lafrasse S., Duvert G., Chelli A., Le Bouquin J.-B., Delfosse X., Chesneau O., 2017, VizieR Online Data Catalog, 2346

Casagrande L., VandenBerg D. A., 2018, MNRAS, 479, L102

Chelli A., Duvert G., Bourgès L., Mella G., Lafrasse S., Bonneau D., Chesneau O., 2016, A&A, 589, A112

Cohen M., Walker R. G., Carter B., Hammersley P., Kidger M., Noguchi K., 1999, AJ, 117, 1864

Cutri R. M. et al., 2003, 2MASS All Sky Catalog of Point Sources, Infrared Science Archive. NASA/IPAC, United States

Cutri R. M. et al., 2012, Technical Report, Explanatory Supplement to the WISE All-Sky Data Release Products. NASA Technical Report Server, United States

Cutri R. M. et al., 2013, Technical Report, Explanatory Supplement to the AllWISE Data Release Products. NASA Technical Report Server, United States

Duvert G., 2016, VizieR Online Data Catalog, 2345

Egan M. P., Price S. D., Kraemer K. E., 2003, American Astronomical Society Meeting Abstracts, #57.08

ESA, 1997, The HIPPARCOS and TYCHO Catalogues. Astrometric and Photometric Star Catalogues Derived from the ESA HIPPARCOS Space Astrometry Mission. Noordwijk, Netherlands

Gaia Collaboration, 2018, A&A, 616, A1

Hall R. T., 1974, A Catalog of 10 Micrometer Celestial Objects. NASA STI, United States

Helou G., Walker D. W., 1988, Infrared Astronomical Satellite (IRAS), Catalogs and Atlases. Vol. 7. The Small Scale Structure Catalog. NASA RP-1190

Høg E. et al., 2000, A&A, 355, L27

Ishihara D. et al., 2010, A&A, 514, A1

Leinert C. et al., 2003, Ap&SS, 286, 73

Lopez B. et al., 2014, The Messenger, 157, 5

Luri X. et al., 2018, A&A, 616, A9

Mason B. D., Wycoff G. L., Hartkopf W. I., Douglass G. G., Worley C. E., 2001, AJ, 122, 3466

McDonald I., Zijlstra A. A., Watson R. A., 2017, MNRAS, 471, 770

Morel M., Magnenat P., 1978, A&AS, 34, 477

Moshir M. et al., 1990, BAAS, 22, 1325

Paresce F. et al., 1996, The Messenger, 83, 14

Robbe-Dubois S. et al., 2018, in Creech-Eakman M. J., Tuthill P. G., Mérand A., eds, Proc. SPIE Conf. Ser. Vol. 10701, Optical and Infrared Interferometry and Imaging VI. SPIE, Bellingham, p. 107010H

Smith B. J., Price S. D., Baker R. I., 2004, ApJS, 154, 673

ten Brummelaar T. A. et al., 2005, ApJ, 628, 453

Verhoelst T., 2005, PhD thesis, K.U. Leuven

Wenger M. et al., 2000, A&AS, 143, 9

Wright E. L. et al., 2010, AJ, 140, 1868

Wu C.-J., Wu H., Lam M.-I., Yang M., Wen X.-Q., Li S., Zhang T.-J., Gao L., 2013, ApJS, 208, 1

SUPPORTING INFORMATION

Supplementary data are available at *MNRAS* online.

table12_hybrid_ATfaint+_excfree.txt

Please note: Oxford University Press is not responsible for the content or functionality of any supporting materials supplied by the authors. Any queries (other than missing material) should be directed to the corresponding author for the article.

APPENDIX A: USED CATALOGUES

Table A1 lists all the catalogues used to build the MDFC catalogue, with some of their general features: VizieR reference, title, number of entries, and main reference.

Downloaded from https://academic.oup.com/mnras/article/490/3/3158/5583026 by guest on 10 February 2023

Table A1. Catalogues and lists used to build the MDFC catalogue.

Catalogue/list	Title	# of entries	Ref.
SIMBAD	The SIMBAD/CDS data base	8230 006	Wenger et al. (2000)
I/239/tyc_main	The *Hipparcos* and Tycho Catalogues	1058 332	ESA (1997)
I/345/gaia2	*Gaia* data release 2 (DR2)	1692 919 135	Gaia Collaboration (2018)
I/347/gaia2dis	Estimating distances from *Gaia* DR2 parallaxes	331 909 727	Bailer-Jones et al. (2018)
II/7A/catalog	*UBVRIJKLMNH* Photoelectric Catalogue	5943	Morel & Magnenat (1978)
II/53/catalog	Catalogue of 10-micron Celestial Objects	647	Hall (1974)
II/125/main	*IRAS* catalogue of Point Sources, Version 2.0	245 889	Helou & Walker (1988)
II/156A/main	*IRAS* Faint Source Catalogue, $\|b\| > 10$, Version 2.0	173 044	Moshir et al. (1990)
II/246/out	2MASS All-Sky Catalogue of Point Sources	470 992 970	Cutri et al. (2003)
II/293/glimpse	GLIMPSE Source Catalogue (I + II +3D)	104 240 613	Benjamin et al. (2003)
II/297/irc	AKARI/IRC mid-IR all-sky Survey	870 973	Ishihara et al. (2010)
II/311/wise	*WISE* All-Sky Data Release	563 921 584	Wright et al. (2010)
II/328/allwise	AllWISE Data Release	747 634 026	Idem
II/338/catalog	*IRAS* PSC/FSC Combined Catalogue	345 162	Abrahamyan et al. (2015)
II/345/jmdc	JMMC Measured Stellar Diameters Catalogue	1554	Duvert (2016)
II/346/jsdc_v2	JMMC Stellar Diameters Catalogue	465 877	Bourgès et al. (2017)
V/114/msx6_gp	The complete MSX6C catalogue in the Galactic Plane ($\|b\| \leq 6^\circ$)	431 711	Egan et al. (2003)
V/114/msx6_main	MSX6C Infrared Point Source Catalogue, High latitude, $\|b\| > 6$	10 168	Idem
B/wds/wds	Washington Double Star Catalogue	142 596	Mason et al. (2001)
J/ApJS/154/673/DIRBE	*COBE* DIRBE Point Source Catalogue	11 788	Smith et al. (2004)
J/MNRAS/471/770/table1	Param. and IR exc. of *Gaia* DR1 stars. Tycho-Gaia astrom. solution	1475 921	McDonald et al. (2017)
J/MNRAS/471/770/table2	Param. and IR exc. of *Gaia* DR1 stars. *Hipparcos*-Gaia astrom. solution	107 110	Idem
J/MNRAS/471/770/table3	Param. and IR exc. of *Gaia* DR1 stars. Stars with IR excess	4255	Idem
mcc.txt[a]	VLTI/MIDI list of calibrator candidates	403	Verhoelst (2005)
980440.tb400.txt[b]	Stars with calibrated spectral templates	422	Cohen et al. (1999), Table 4
Cohen_list.html[c]	Complete set of Cohen's standards	435	Gemini Obs. (MIR Resources)

Notes. [a]http://ster.kuleuven.be/~tijl/MIDI_calibration/mcc.txt
[b]https://iopscience.iop.org/article/10.1086/300813/fulltext/980440.tb400.txt
[c]www.gemini.edu/sciops/instruments/mir/Cohen_list.html

APPENDIX B: TABLE COLUMNS

Table B1 describes the columns reported in the catalogue.

Downloaded from https://academic.oup.com/mnras/article/490/3/3158/5583026 by guest on 10 February 2023

Table B1. Description of the catalogue fields.

Label	Units	Explanations
Name		SIMBAD main identifier
SpType		SIMBAD spectral type
RAJ2000	'h:m:s'	Barycentric right ascension (ICRS) at Ep = 2000.0
Dec.J2000	'd:m:s'	Barycentric declination (ICRS) at Ep = 2000.0
Distance	pc	Estimated distance from Bailer-Jones et al. (2018)
teff_midi	K	Estimate of effective temperature from VLTI/ MIDI
teff_gaia	K	Estimate of effective temperature[a] from Gaia DR2 (from Apsis-Priam, see Andrae et al. 2018)
Comp		Components when more than 2 from WDS
mean_sep	'	Mean separation from WDS
mag1	mag	Magnitude of First Component from WDS
mag2	mag	Magnitude of Second Component from WDS
diam_midi	mas	Fitted angular diameter from VLTI/MIDI
e_diam_midi	mas	Error on VLTI/MIDI angular diameter
diam_cohen	mas	Fitted angular diameter from Cohen et al. (1999)
e_diam_cohen	mas	Error on Cohen's angular diameter
diam_gaia	mas	Estimate of angular diameter from Gaia DR2[a]
LDD_meas	mas	Measured LDD angular diameter from JMDC
e_diam_meas	mas	Error on measured angular diameter from JMDC
UDD_meas	mas	Measured UD angular diameter from JMDC
band_meas		Text describing the wavelength or band of the angular diameter measurement from JMDC
LDD_est	mas	Estimated LDD angular diameter from JSDC_V2
e_diam_est	mas	Error on estimated angular diameterfrom JSDC_V2
UDDL_est	mas	Estimated UD angular diameter in *L* from JSDC_V2
UDDM_est	mas	Estimated UD angular diameter in *M* from JSDC_V2
UDDN_est	mas	Estimated UD angular diameter in *N* from JSDC_V2
Jmag	mag	2MASS *J* magnitude (1.25 μm)
Hmag	mag	2MASS *H* magnitude (1.65 μm)
Kmag	mag	2MASS *Ks* magnitude (2.17 μm)
W4mag	mag	AllWISE W4 magnitude (22.1 μm)
CalFlag		[0/7] Confidence flag for using this star as a calibrator in Opt. Interf. experiments from JSDC_V2
IRflag		[0/7] Confidence flag indicating the probable presence of MIR features (excess, extent, variability)
nb_Lflux		Number of flux values reported in *L*
med_Lflux	Jy	Median flux value in *L*
disp_Lflux	Jy	Dispersion of flux values in *L*
nb_Mflux		Number of flux values reported in *M*
med_Mflux	Jy	Median flux value in *M*
disp_Mflux	Jy	Dispersion of flux values in *M*
nb_Nflux		Number of flux values reported in *N*
med_Nflux	Jy	Median flux value in *N*
disp_Nflux	Jy	Dispersion of flux values in *N*
Lcorflux_30	Jy	Uniform-disc correlated flux in *L* for 30-m baselength
Lcorflux_100	Jy	Uniform-disc correlated flux in *L* for 100-m baselength
Lcorflux_130	Jy	Uniform-disc correlated flux in *L* for 130-m baselength
Mcorflux_30	Jy	Uniform-disc correlated flux in *M* for 30-m baselength
Mcorflux_100	Jy	Uniform-disc correlated flux in *M* for 100-m baselength
Mcorflux_130	Jy	Uniform-disc correlated flux in *M* for 130-m baselength
Ncorflux_30	Jy	Uniform-disc correlated flux in *N* for 30-m baselength
Ncorflux_100	Jy	Uniform-disc correlated flux in *N* for 100-m baselength
Ncorflux_130	Jy	Uniform-disc correlated flux in *N* for 130-m baselength

Notes. [a]The values of teff_gaia and diam_gaia were determined only from the three broad-band photometric measurements used with *Gaia*. The strong degeneracy between $T_{\rm eff}$ and extinction/reddening when using the broad-band photometry necessitates strong assumptions in order to estimate their values (see e.g. Casagrande & VandenBerg 2018). One should thus be very careful in using these astrophysical parameters and refer to the papers and online documentation for guidance.

This paper has been typeset from a TEX/LATEX file prepared by the author.

Downloaded from https://academic.oup.com/mnras/article/490/3/3158/5583026 by guest on 10 February 2023